J. Fluid Mech. (1992), *vol.* 241, *pp.* 371–402
Printed in Great Britain

Vortex structure and dynamics in the near field of a coaxial jet

By WERNER J. A. DAHM[1], CLIFFORD E. FRIELER[2] AND GRÉTAR TRYGGVASON[3]

[1] Department of Aerospace Engineering, The University of Michigan, Ann Arbor, MI 48109–2140, USA

[2] Graduate Aeronautical Laboratories, California Institute of Technology, Pasadena, CA 91125, USA

[3] Department of Mechanical Engineering & Applied Mechanics, The University of Michigan, Ann Arbor, MI 48109–2125, USA

(Received 20 February 1990 and in revised form 3 January 1992)

We present results from an experimental and numerical investigation into the structure of vortex patterns and the dynamics of their interactions for the incompressible flow in the near field of a round coaxial jet issuing into a quiescent ambient fluid. A two-colour planar laser-induced-fluorescence technique is used to document the flow field via still photographs and ciné sequences over a limited range of parameters. We examine the effects of varying the velocity ratio as well as the absolute velocities of the two coaxial streams for equal densities and for a single area ratio. Results show that a variety of widely differing near-field vortex patterns can arise, with very different interaction dynamics, which can depend both on the velocity ratio and on the absolute velocities of the two streams. The observed vortex structures and their dynamics are interpreted in terms of the instability of the initially cylindrical and concentric vorticity layers separating each of the fluid streams, and their subsequent rollup to form wake-like or shear-layer-like vortices. Our results show that in addition to the velocity jump across each of these vorticity layers, an accounting of the layer thicknesses and the wake defect within each layer can be essential to understanding the resulting near-field structure that occurs. Ensuing dynamical interactions between the vortices formed from each layer can produce a strong coupling between the development of the two layers. These resulting vortex structures and interaction dynamics are also seen to produce widely differing mixing patterns in the jet near field.

1. Introduction

The near field of coaxial jets, typically extending over the first two or three diameters beyond the jet exit, has been a subject of investigation for more than twenty years. Much of this interest can be traced to reductions in flow noise achievable with such coaxial jets in comparison with simple jets. Classically, the noise produced has been formulated in terms of an analogy (Lighthill 1952) in which the acoustic far field generated by a low-Mach-number flow is expressed in terms of an equivalent distribution of local quadrupole sources with strengths determined by $(\partial^2/\partial x_i \partial x_j)\rho_0 u_i u_j$. In practice, however, strict application of Lighthill's formulation requires a level of detailed information about the instantaneous velocity field that is rarely available. As a consequence, its application to practical problems almost

always requires resort to *ad hoc* arguments relating the source strengths to, for example, the mean flow field and its turbulent fluctuations. This approach has nevertheless led to an understanding of some of the parameters controlling fluid dynamic noise generation. For instance, scaling arguments based on this formulation, summarized by Lighthill (1954, 1963), indicate that much of the noise produced by simple turbulent jets originates from roughly the first four diameters downstream of the jet. Arguments of this type, however, rely crucially on empirical information about the flow in the jet near field. Further, such semiempirical arguments suggest that, at Mach numbers below about two, the noise generated by the simple jet near field, for a given thrust, increases with the sixth power of the jet exit velocity. This result has been interpreted as suggesting that a primary means for reducing the noise generated by jets is to decrease the exit velocity. As a practical example, this reasoning has been one of the motivations behind the use of high-bypass jet engines to reduce the noise generated in aircraft propulsion. Yet it has been empirically observed that the noise produced by such simple jets, for a fixed exit velocity, can actually be reduced by the addition of a surrounding coaxial stream. Indeed, the combined noise of such an arrangement has been shown (e.g. Williams, Ali & Anderson 1969; Dosanjh, Yu & Abdelhamid 1971) to be lower than that of the original inner jet alone. Motivated by such observations, Olsen & Friedman (1974) have empirically documented variations in noise emitted by the near field of such a coaxial jet flow for various velocity ratios and exit area ratios. Other measurements (e.g. Tanna & Dean 1975) show further effects of the coaxial stream temperatures on the noise generated by the near field. While there has been some success in correlating these observed noise characteristics of the near field of coaxial jets with various implementations of Lighthill's acoustic formulation (e.g. Balsa & Gliebe 1977), these also rely heavily on *ad hoc* arguments and empirical information about the velocity field. Although these can provide useful engineering approximations, they provide only very limited insight into the underlying noise generation mechanisms and into innovative noise reduction strategies for such flows.

An alternative formulation of *vortex* sound in low-Mach-number flows was originally proposed by Powell (1964), and later formalized by Howe (1975), in which the acoustic far field is expressed in terms of a distribution of local dipole sources with strengths $\rho_0 \nabla \cdot (\boldsymbol{\omega} \times \boldsymbol{u})$, where $\boldsymbol{\omega} \equiv \nabla \times \boldsymbol{u}$ is the vorticity. This formulation is in some respects more attractive than the classical acoustic analogy because it provides a more physically intuitive and dynamically insightful identification of the noise sources. Möhring (1978) introduces yet an entirely different integral formulation for low-Mach-number flows that goes further and directly expresses the acoustic far field in terms of the vorticity field alone. From this, Möhring has derived the sound field generated by an isolated vortex ring, as well as that due to a pair of coaxial, interacting (i.e. 'leapfrogging') vortex rings. In both these formulations, it is the vorticity that is the basic element producing both the flow field and the acoustic far field. This suggests that the noise generated by both simple and coaxial jets might be usefully viewed from the perspective of the large-scale vortical structure in the near field of each of these flows. Indeed, it further suggests possibilities for eventually controlling the noise generated by such jets through control of their near-field vortex structure and dynamics.

In simple jets, this large-scale vortical structure of the near field has been fairly well established in terms of the instability of a cylindrical vortex sheet (Michalke & Hermann 1982) and its subsequent rollup to form vortex rings and helixes (e.g. Becker & Massaro 1968; Beavers & Wilson 1970; Crow & Champagne 1971; Yule

1973). By comparison, in coaxial jets very little is known about the underlying near-field vortex structure or its dynamics, and in particular how this near-field structure depends on the stream velocities. Most investigations of coaxial jets to date have been restricted to measurements of time-averaged velocity profiles, turbulence quantities and pressure spectra (e.g. Chigier & Beer 1964; Williams *et al.* 1969; Champagne & Wygnanski 1971; Ribeiro & Whitelaw 1980). These have not, however, addressed the vortex structure of the flow field which ultimately produces these characteristics of the flow. Perhaps the most extensive investigations are by Ko & Kwan (1976) and Kwan & Ko (1977), and for the special case of the annular jet by Ko & Chan (1978, 1979) and Chan & Ko (1978), in which they specifically attempt to infer this near-field vortex structure from pressure and velocity measurements. From their results, they view the coaxial jet near field as consisting of two concentric trains of vortex rings, and interpret their measurements as showing that successive rings in each train are equally spaced at 1.2 times their respective exit diameters (e.g. see figures 1 and 2 of Kwan & Ko 1977). They further interpret their results as suggesting that the interaction between the vortex rings from these two trains depends on the velocity ratio of the two coaxial streams, and draw the overall conclusion that the vortex structure in the near field of coaxial jets can be described simply as a combination of the near-field structures of two simple jets. More recently, Wlezian & Kibens (1985) have also made some early attempts at correlating the noise characteristics for the special case of an annular jet with its shear-layer dynamics. However, at present no clear understanding exists for the underlying near-field vortex structure and dynamics of such coaxial jets, or of how this near-field structure varies with the stream velocities.

In this paper we attempt to provide a clearer physical picture of the structure of vortex patterns and the dynamics of their interactions in the coaxial jet near field. We concentrate on the incompressible flow in the near field of such a jet and examine effects of varying the two coaxial stream velocities for equal densities and a single area ratio. The emphasis is principally on documenting the structure and variety of near-field patterns and dynamics that occur, and identifying how these depend on various characteristics of the flow at the jet exit. We use a two-colour planar laser-induced-fluorescence technique to follow the instability and rollup of the initially concentric and cylindrical vorticity layers at the two interfaces separating the inner, annular and ambient streams. The presentation is organized as follows. In §2 we give a brief overview of the coaxial jet apparatus used for these experiments and the two-colour planar laser-induced-fluorescence technique. In §3 we summarize the instability and initial rollup modes of the compound velocity profiles that result at the jet exit. Results for the near-field vortex structure and dynamics over a range of the coaxial stream velocities are presented in §4 together with a discussion of some of these results. We draw conclusions in §5. In addition, a discussion of shear-layer vortex interactions relevant to our arguments concerning a locking between the two layers is given in the Appendix.

2. Experimental procedure

The experiments were conducted using water in a tank with $33 \times 33 \times 62$ in. interior dimensions and with 31×31 in. windows on four sides. The two coaxial streams discharged from a pair of concentric plena into the quiescent ambient fluid through a concentrically arranged pair of contoured axisymmetric nozzles with coplanar exits. The nozzle contours are shown to scale in figure 1. At the exit plane,

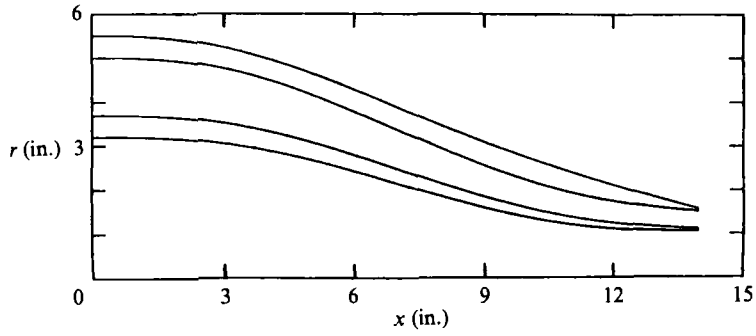

FIGURE 1. The axisymmetric nozzle contours used in these experiments, shown to scale. The nozzles were numerically machined to follow a family of polynomial shapes designed to avoid the formation of Görtler vortices in the contraction section.

the outer nozzle had a 3.01 in. interior diameter, while the inner nozzle had an interior diameter of 2.10 in. and a 0.05 in. wall thickness, giving the nozzle exit diameter ratio as 1.40 and the annular-to-inner nozzle exit area ratio as 0.94. As shown schematically in figure 2, the two fluids were discharged through these coaxial nozzles by controlling their plenum free-surface elevation above the reservoir level with separate nitrogen streams issuing through a pair of micrometer-controlled variable-throat metering orifices held at sonic conditions with a constant upstream pressure of 60 p.s.i. Two solenoid valves, one in each circuit, were opened in unison to initiate the flow. Table 1 lists the coaxial stream exit velocities in each of the cases for which results are presented in §4.

As can be seen from figure 1, the inner stream experienced a 9.9:1 contraction ratio in going from the plenum to the nozzle exit, while the contraction ratio for the annular stream was 10.6:1. Moreover, the nozzle contours were designed so that the flow along both the inner and outer walls of the annular stream, as well as the flow in the inner nozzle, was continually subjected to favourable pressure gradients. Estimates of the resulting boundary-layer development along the plenum and nozzle walls, using the axisymmetric Thwaites' method together with Michel's method (see White 1974), indicated that the boundary layers remained thin, laminar, and attached in all cases, and provided the estimates given in table 1 for the resulting displacement and momentum thicknesses at the nozzle exit.

An important consideration in such a pressure-driven discharge system is that the spectral content of the impulsive pressure rise driving each stream as the flow is started can excite oscillations at the natural frequency of the second-order system formed by the compressibility of the air and the liquid mass in each circuit. The resulting oscillatory component in the exit velocity of each stream might then impose a forced response on the shear layers formed at the nozzle exit. To avoid such resonant oscillations, we suppressed high frequencies in the pressure rise with the fluid equivalent of a low-pass filter in each drive circuit by placing a resistance in series and an adjustable volume of air in parallel with each plenum. These are also shown schematically in figure 2. The rolloff frequency for each filter was tuned to effectively suppress oscillations at the natural frequency of that circuit. Laser velocimetry measurements confirmed that the two resulting coaxial streams were essentially free of such resonance-driven oscillations. To demonstrate this, figure 3(*a*) shows the measured result for the variation with time in exit velocity of the inner stream in

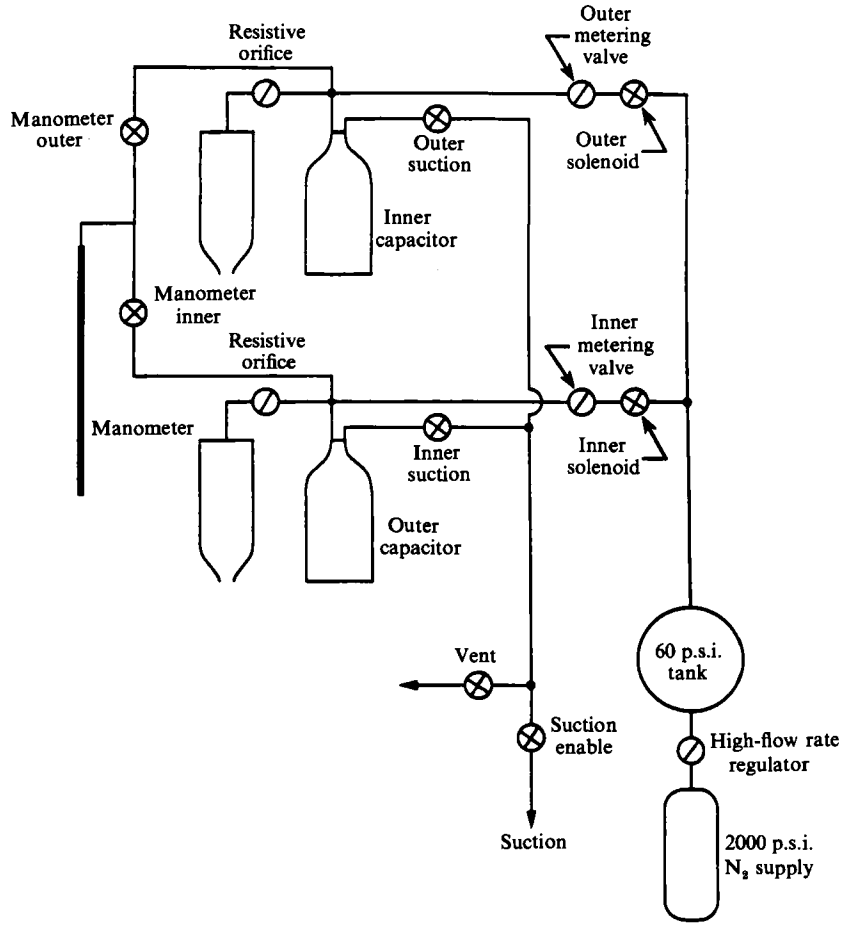

FIGURE 2. Schematic representation of the pneumatic drive system used to control the two coaxial stream velocities as described in §2. Note especially the fluid capacitor and resistive orifice in each drive circuit for spectrally filtering the pressure rise to avoid exciting the natural frequency of each plenum and nozzle. The inner and outer plena and nozzles are actually concentrically arranged.

response to the essentially impulsive pressure rise that occurs without any such filter in the drive circuit. In this case the plenum was only half-filled, so the amplitude of the oscillations is very large, with the resulting natural frequency approximately 3.3 Hz. Figure 3(*b*) shows the same arrangement after the addition of the low-pass filter, but before the filter has been completely tuned. Notice that the amplitude of the oscillations has been considerably reduced. Finally, figure 3(*c*) shows the result after the filter has been optimally tuned for this configuration. Notice that, even in this extreme case, there are no discernible remaining oscillations at the natural frequency. More typically, with the plena completely filled at the start of each experiment, the rise times achieved are considerably shorter than that in figure 3(*c*), and are generally around 0.5 s. Note also that the slight decrease in exit velocity apparent in figure 3 with increasing time is due to the decreasing hydrostatic head as the free surface in the plenum drops. Over the duration of a typical experiment this effect was negligible.

The resulting vortex structure in the near field was visualized with a two-colour

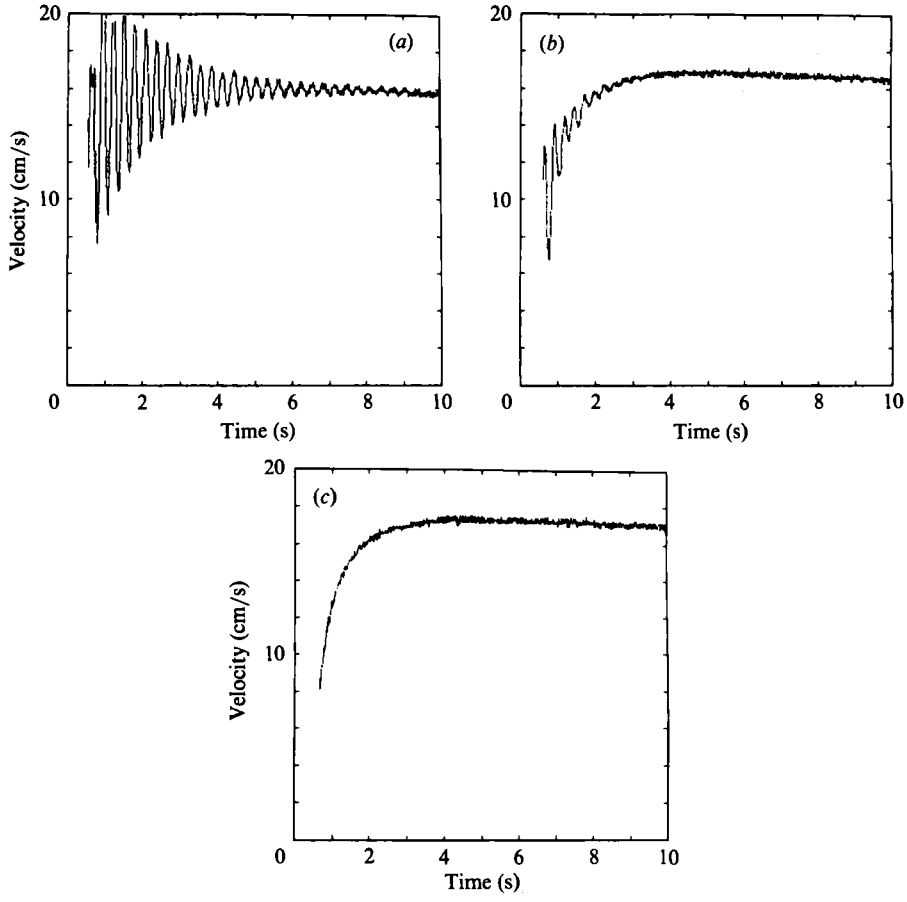

FIGURE 3. Laser velocimetry measurements of the exit velocity for one of the coaxial streams showing the response of the fluid system to an impulsive pressure rise for varying levels of low-pass filtering (see §2). Even in this extreme case, note that oscillations at the natural frequency can be effectively suppressed. (*a*) No low-pass filter, (*b*) partially tuned low-pass filter, (*c*) fully tuned low-pass filter.

planar laser-induced-fluorescence (LIF) technique and recorded with still and ciné photography. The fluid originating from each of the coaxial streams was marked with a different laser-fluorescent dye, and the near field illuminated in a diametral plane by a thin laser sheet formed from a 3W argon ion laser. The inner fluid (referred to as stream 1) consisted of an aqueous solution of Rhodamine B, which fluoresces red, while the annular fluid (referred to as stream 2) was an aqueous solution of disodium fluorescein, which fluoresces yellow. Each of the dye concentrations, typically 10^{-6} M, was sufficiently weak as to have no effect on the density. Using an orange filter to block any directly scattered laser light, we recorded the fluorescence from both fluids in the plane of the laser sheet on 35 mm colour slide film and 16 mm colour ciné film at 60 frames/s over a range of values for the two coaxial stream velocities. In the photographic prints presented in §4, the inner fluid appears grey and the annular fluid appears white. The ambient fluid (stream 3) contained no dye and appears black in these photographs. Here we use the grey–white and white–black dye interfaces to mark the instability, subsequent rollup, and mutual interaction of

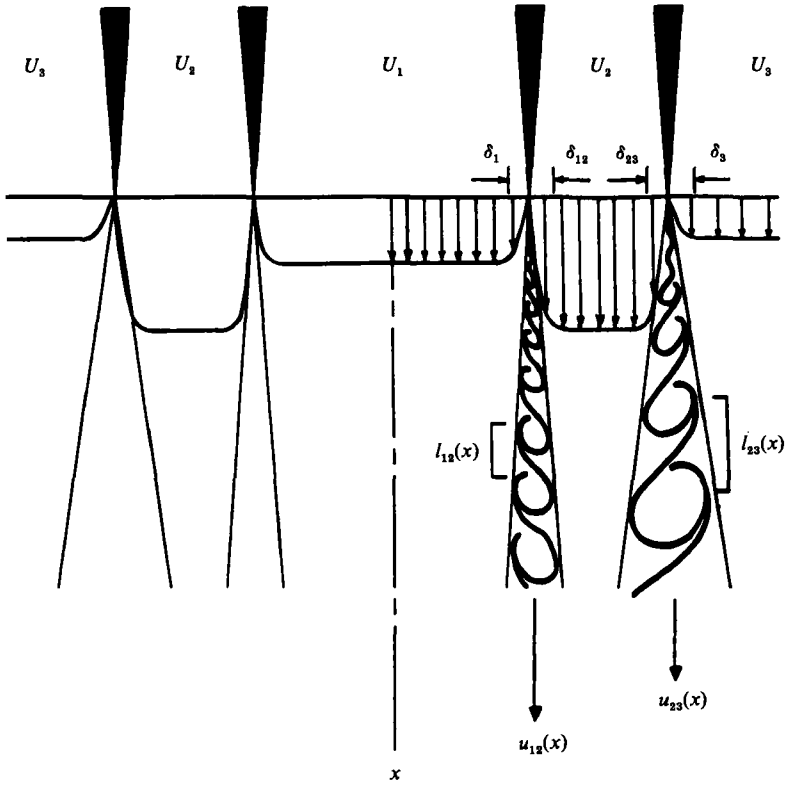

FIGURE 4. Schematic representation of a typical velocity profile at the jet exit, including the velocity defects imparted by the viscous boundary layers along the nozzle walls. Table 1 gives the values of the coaxial stream velocities used and estimates of the resulting laminar boundary-layer thicknesses for each of the cases presented in §4. Shown here is the general case ($U_3 \neq 0$); the present experiments are confined to $U_3 = 0$.

the two thin and initially cylindrical vorticity layers separating the streams at the nozzle exit. Of course, since the vorticity diffuses faster than the dye (the Schmidt number is large), far enough downstream these dye interfaces will no longer be a meaningful marker of the vorticity field. However, our attention is focused here on the near field, and the interfaces certainly provide a useful indication of the evolution of these vortex sheets over the first few jet diameters.

3. Instability and initial rollup modes

Figure 4 schematically shows the typical exit velocity profile across the two interfaces separating the three coaxial streams. Between each pair of streams, there is a velocity jump resulting from the difference in stream velocities together with a velocity defect imparted by the viscous boundary layers on either side of each nozzle lip. It is useful to conceptually view this compound velocity profile as being composed of a wake component and a shear-layer component resulting, respectively, from the symmetric and antisymmetric parts of the profile, as indicated in figure 5. If the wake component vanishes, then the natural instability of the resulting velocity profile would closely correspond to the shear-layer instabilities calculated by Michalke (1964) for the hyperbolic tangent profile, and will subsequently roll up to

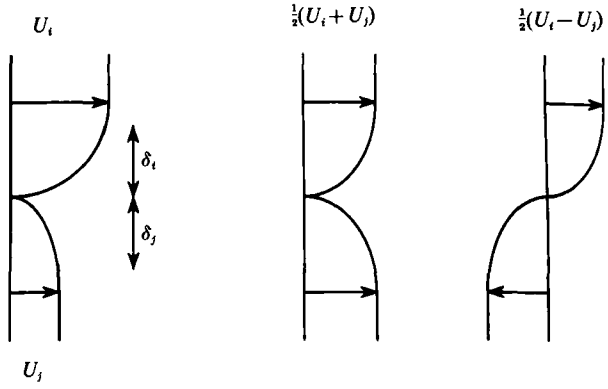

FIGURE 5. Conceptual decomposition of a typical velocity profile (left) at the nozzle exit into a wake component (centre) and a shear-layer component (right), corresponding respectively to the symmetric and antisymmetric parts of the profile. The instability and the subsequent rollup of the interface that results from such a compound velocity profile is termed 'wake-like' if dominated by vorticity concentrations with both signs of circulation, and 'shear-layer-like' if dominated by vortices with just one sign of circulation.

form concentrations of vorticity dominated by just one sign of circulation. On the other hand, if the velocity jump across the interface is zero, then the natural evolution of the velocity defect imparted by the boundary layers on either side of the nozzle lip will develop a wake instability (Mattingly & Criminale 1972). In that case two different modes of instability are possible, with the dominant one subsequently rolling up to form a staggered array of vorticity concentrations with opposing signs of circulation (Mode I in the notation of Mattingly & Criminale). In general, both the wake and the shear-layer components will be present, and the resulting instability is more complex. Miksad (1972) has shown that the temporal instability of such compound velocity profiles also admits two modes of evolution. For the spatial stability of such profiles, Koochesfahani & Frieler (1989) have further confirmed the presence of two modes, and have shown that their mode 1 is always more unstable if the two streams have equal densities (but also show that the second mode can actually become more unstable if the density ratio between the two streams is made large enough). They further demonstrate that the eigenfunction corresponding to the most unstable disturbance in this mode produces the shear-layer and wake rollup patterns as the two limiting cases described above are approached. For the rollup that results from an arbitrary profile of the type indicated in figure 5, the eigenfunction corresponding to the most unstable disturbance could result in an initial rollup pattern that more nearly resembles the shear-layer rollup mode or the wake rollup mode, but in general could be significantly different from either of these. Here we will broadly refer to the rollup patterns that evolve from such compound velocity profiles as 'shear-layer-like' if they are dominated by vorticity concentrations with just one sign of circulation, and as 'wake-like' those that are dominated by vortices with opposing signs (but possibly unequal magnitudes) of circulation.

If the vortex formation and evolution in the two concentric layers were to proceed independently of each other then, for those cases in which both layers form shear-layer-like vortices, estimates of the near-field vortex properties might be obtained from the scaling laws for a single, isolated shear layer. From a dynamical perspective, the vortex passage frequency ratio and circulation ratio would appear to be among

Case	U_1 (cm/s)	U_2 (cm/s)	U_3 (cm/s)	U_2/U_1	δ_1 (cm)	δ_{12} (cm)	δ_{23} (cm)	θ_1 (cm)	θ_{12} (cm)	θ_{23} (cm)	Figure
1	11	6.5	0	0.59	0.127	0.110	0.108	0.051	0.048	0.050	6
2	11	7.8	0	0.71	0.127	0.101	0.099	0.051	0.044	0.046	7
3	11	11	0	1.00	0.127	0.085	0.083	0.051	0.037	0.038	8, 12
4	11	12.5	0	1.14	0.127	0.080	0.078	0.051	0.035	0.036	9
5	11	28.1	0	2.56	0.127	0.053	0.052	0.051	0.023	0.024	10
6	2.5	10.4	0	4.16	0.266	0.087	0.085	0.107	0.038	0.039	11
7	20	20	0	1.00	0.094	0.053	0.052	0.038	0.023	0.024	12, 13

TABLE 1. Experimental conditions in figures 6–13. The laminar boundary-layer displacement thickness δ and momentum thickness θ listed are axisymmetric Thwaites' method estimates for the geometry shown in figure 1.

the most important quantities in determining the resulting near-field vortex interactions. Both of these can be estimated from the scaling laws for an isolated shear layer. Such an analysis is given in the Appendix, and in the results that follow we compare these predicted frequency ratios with the observed ones to assess, in part, the extent to which the two layers develop independently.

Of course, since the initial instability and subsequent rollup at each interface occur quite close to similar processes occurring at the other interface, it seems likely that the two layers might not develop entirely independent of each other. Instead, vortices formed at one interface and their interactions with those at the other interface might very well excite an instability other than the naturally dominant one in the vorticity layers at the nozzle exit. The instability and rollup processes in the two concentric layers may then 'lock' into each other in this manner. Moreover, the ensuing evolution of the vortices formed from each layer may also be affected by the presence of the vortices in the other layer. Indeed, clear indications can be seen of such locking in the vortex formation and evolution between the two layers in some of the results presented in the following section.

4. Results and discussion

Figures 6–13 show typical results for the vortex structure and dynamics in the coaxial jet near field over a range of values of the two stream velocities. Table 1 summarizes the conditions for each of the cases shown. It is essential to note that the precise near-field vortex patterns observed are inherently time-dependent, but essentially periodic. For this reason, in each case the ciné films give the best appreciation for the range of vortex patterns and their dynamics that result in the jet near field. To convey this information, we typically show a single still photograph giving a detailed view of the characteristic vortex structure for each case, together with a composite time sequence from the ciné film data to give an indication of the resulting vortex dynamics in the rear field. Each of these composite sequences is a single contiguous time series of 21 successive photographs equally spaced in time, constructed from every fifth frame of a segment of the ciné film data. For the framing rate used, the resulting temporal separation between successive photographs in each of these time series is 83 ms for all of the cases shown. In each sequence, time increases from left to right, and then from top to bottom. These composite sequences allow dynamical interactions among the vortices to be seen, while the more highly resolved still photographs give a better view of the typical instantaneous vortex

(a)

FIGURE 6(a). For caption see facing page.

structure. In the discussion that follows, we examine separately some effects of the velocity ratio and the absolute stream velocities on the near-field vortex structure and dynamics apparent in these data.

4.1. *Effect of velocity ratio*

Figures 6–11 show the near-field vortex structures and the dynamics of their interactions for increasing values of the outer-to-inner-stream velocity ratio, U_2/U_1. The ambient fluid velocity U_3 is zero in all cases. Note that the inner stream velocity U_1 is held constant at 11 cm/s in figures 6–10, while the outer stream velocity U_2 is systematically increased to vary the velocity ratio. This has the effect of holding the laminar boundary-layer thickness δ_1 on the inside wall of the inner nozzle fixed, while gradually decreasing the layer thicknesses δ_{12} and δ_{23} at the inner and outer walls of the annular stream. In the context of the discussion in §3, the result is that in going from figures 6 to 10 the width of the velocity *defect* which these boundary layers impart on each of the two shear-layer velocity profiles at the nozzle exit gradually decreases, and the magnitude of this velocity deficit gradually increases. On the other hand, the magnitude of the velocity *jump* U_2-U_3 across the outer shear layer continually increases in going from figures 6 to 11, while the magnitude of the jump U_2-U_1 across the inner layer initially decreases in figures 6 to 8, and then changes sign and increases in figures 8 to 10.

We first examine figure 6 (Case 1 in table 1), for which the velocity ratio $U_2/U_1 = 0.59$. Here the velocity jump across both layers has the same sign and roughly the same magnitude. The outer layer can be seen to initially develop an axisymmetric instability that subsequently develops into a shear-layer-like rollup, in agreement with the jet instability results for hyperbolic tangent profiles in the absence of any wake deficit by Michalke & Hermann (1982). At somewhat larger axial distances, these shear-layer vortices take on a non-axisymmetric form which, in this diametral view, corresponds to a helical vortex structure of the near field. This also appears qualitatively consistent with the result by Michalke & Hermann that a

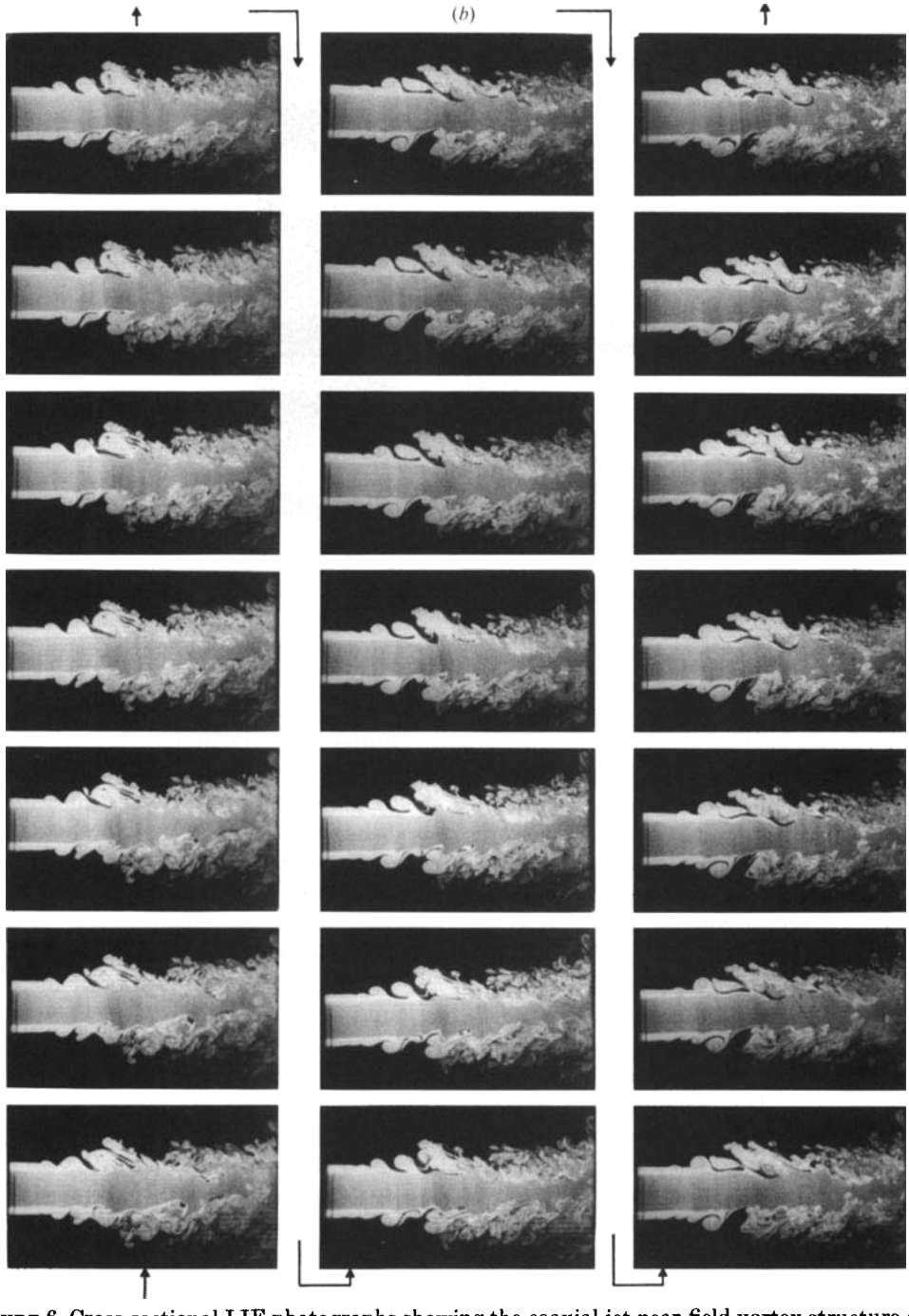

FIGURE 6. Cross-sectional LIF photographs showing the coaxial jet near-field vortex structure and dynamics for $U_2/U_1 = 0.59$ (Case 1 in table 1). In this case, the velocity jump across the two initially concentric vorticity layers is roughly the same, but the inner layer is considerably thicker. As a result, the inner layer is almost dynamically irrelevant, and the near field appears to be dominated by the helical shear-layer-like vortices that form in the outer layer. (*a*) Typical near-field vortex structure. (*b*) A single time sequence showing typical vortex dynamics in the near field. The sequence begins at bottom left, with time increasing from bottom to top of each column, and from left to right, finishing at top right as shown by the arrows.

(*a*)

FIGURE 7(*a*). For caption see facing page.

helical ($m = 1$) mode becomes dominant as the velocity profile smooths out with increasing axial distance (see their figures 1 and 2). The time evolution of this characteristic helical structure can be followed for about the first two diameters downstream in the sequence in figure 6(*b*). By comparison, the inner layer in this case can be best described as lethargic. Perhaps because of its greater thickness (see table 1), whatever instability might occur in it never grows to a sufficient amplitude to show any rollup of the interface before it is dominated by the helical shear-layer vortices in the outer layer. Indeed, the inner interface appears to deform essentially in response to the influences of the vortices in the outer layer, and apparently does not play a major role in determining the near-field vortex structure or dynamics at these conditions. For comparison with the other cases described below, we note that the near field shows a potential core consisting of large, uninterrupted (and therefore presumably irrotational) regions of inner fluid typically extending about six diameters downstream.

Next we turn to figure 7 (Case 2 in table 1) in which the velocity ratio $U_2/U_1 = 0.71$. The velocity jump across both layers still has the same sign, but now differs in magnitude by more than a factor of two. Notice that, despite the rather small change in velocity, in the context of figure 5 the resulting change in velocity jump is significant, and accordingly the near-field structure and dynamics are different than in figure 6. Here, rather than presenting a ciné sequence, we show an ensemble of six detailed views of the near-field structure to give an indication of the range of near-field vortex patterns that result. In this case, although the inner interface begins to show indications of an instability, its subsequent development again appears to be much more strongly dominated by the vortical structures which form in the outer layer than by its own rollup. The outer layer rolls up to form distinct shear-layer-like vortices, which now remain axisymmetric over a much greater distance than in the previous case. This suggests a near-field structure consisting of vortex rings rather than the helical structure in Case 1. The principal dynamical feature in this case appears to be the pairing of these vortex rings,

(*b*)

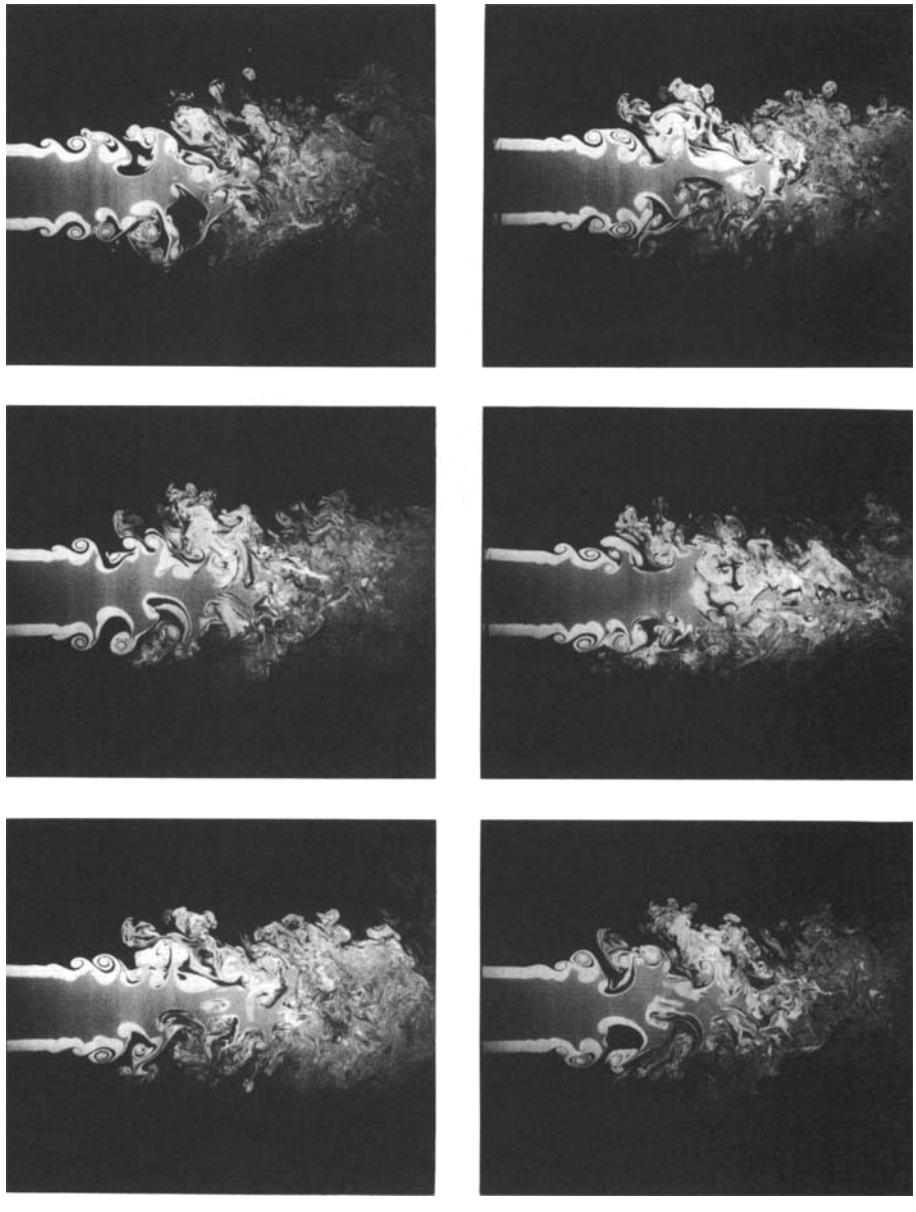

FIGURE 7. Cross-sectional LIF photographs showing the coaxial jet near-field vortex structure for $U_2/U_1 = 0.71$ (Case 2 in table 1). The velocity jump across the outer layer is now more than twice that of the inner layer, and the near-field dynamics are dominated largely by the axisymmetric shear-layer-like vortices that form in the outer layer and their subsequent pairings, which result in a more effective disruption of the potential core than in figure 6 to produce a tentacular appearance. (*a*) Typical near-field vortex structure. (*b*) Several instantaneous realizations of the near-field vortex structure.

consistent with what might be anticipated as an approach to the near-field dynamics of simple jets as $U_2/U_1 \rightarrow 1$. During each such vortex ring pairing, ambient fluid is brought deep into the near field. The resulting penetration of ambient fluid well into the core and the large tongues of inner fluid that are stretched out toward the

(a)

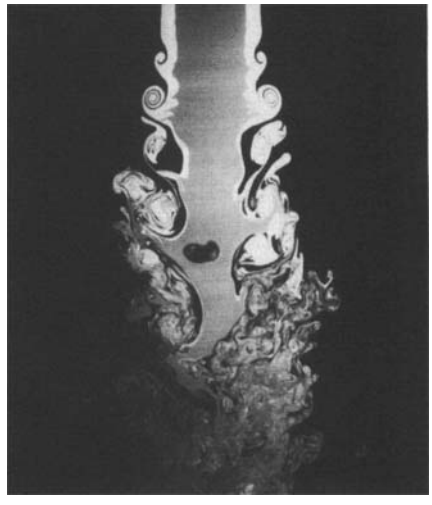

FIGURE 8(a). For caption see facing page.

ambient fluid produces a tentacular appearance in the potential core. Whereas the eventual disintegration of the potential core in Case 1 might be viewed as a gradual 'nibbling' away at its edges, here the core is consumed by just a few large 'bites' resulting from such vortex ring pairings in the outer layer. The resulting potential core in this case is much shorter than in Case 1, and typically reaches only about three diameters beyond the exit.

With the velocity ratio $U_2/U_1 = 1.00$ in figure 8 (Case 3 in table 1), the velocity jump is zero across the inner layer, which now consists only of the wake defect. Correspondingly, a wake-like instability of the inner layer becomes evident, though this instability in the inner layer never has a chance to roll up and form its own distinct vortical structure before interacting with the outer layer. The outer layer again develops into shear-layer-like vortex rings that remain very nearly axisymmetric throughout most of the near field. Overall, the large-scale features of the flow remain remarkably axisymmetric even well into the region where the potential core is being consumed. As in figure 7, it is the pairings that occur among these vortex rings that are principally responsible for the disruption of the potential core. Interestingly, the length of the core is now consistently greater than in figure 7. Perhaps because of the increased symmetry, each of the vortex ring pairings does not reach as far into the core. Note that the case where $U_2/U_1 = 1.00$ is further discussed in §4.2.

We next examine figure 9 (Case 4 in table 1), in which $U_2/U_1 = 1.14$ and accordingly the velocity jumps across the two layers take on opposing signs. Now the instability and subsequent rollup of the inner layer develops to a greater extent before being dominated by the shear-layer vortices in the outer layer. The rollup of the inner layer begins to look more shear-layer-like than wake-like, though the shape of the interface suggests that significant vorticity concentrations with both signs of circulation are still present owing to the strong wake component at the inner interface. The dominant sense of circulation, corresponding to the small velocity jump across the inner layer, just begins to form shear-layer-like vortices when

(*b*)

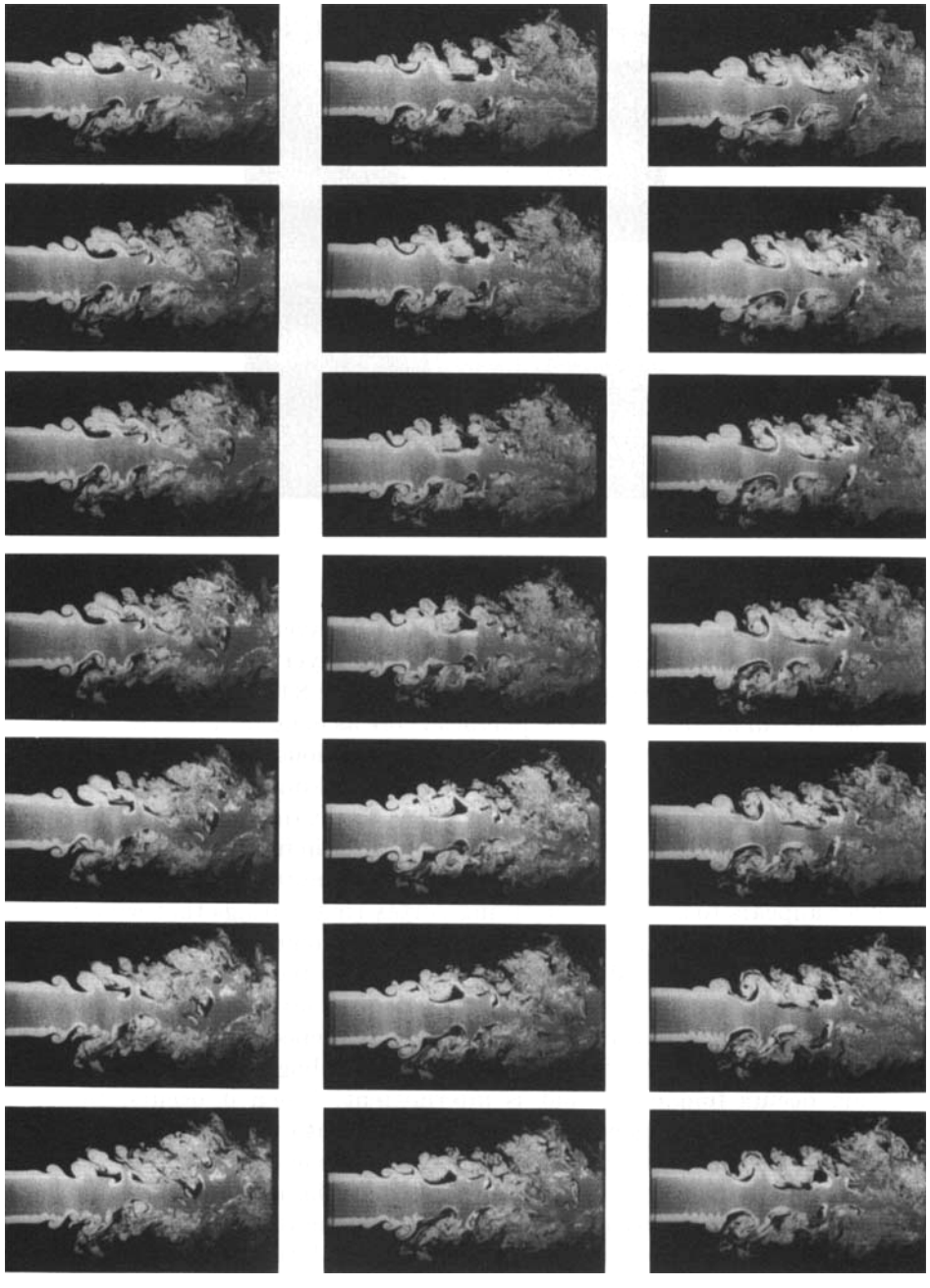

FIGURE 8. Cross-sectional LIF photographs showing the coaxial jet near-field vortex structure and dynamics for $U_2/U_1 = 1.00$ (Case 3 in table 1). Across the inner layer, the velocity jump is now zero, and the layer consists only of the wake defect. The early development of a wake rollup can be seen, but is dominated by the outer-layer vortices before it can develop into dynamically significant vorticity concentrations (see also figures 12 and 13). (*a*) Typical near-field vortex structure. (*b*) Sequence showing typical vortex dynamics in the near field with time increasing from bottom to top, left to right, as in figure 6(*b*).

(a)

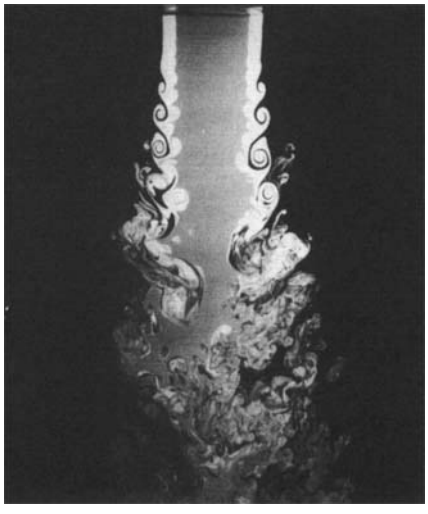

FIGURE 9(a). For caption see facing page.

interactions with shear-layer vortices in the outer layer, which have the opposite sense of circulation, become significant. The outer layer still appears to govern the dynamics through vortex ring pairings, but like figure 8 these pairings do not appear to be as successful in consuming the potential core as in figure 7. Overall the resulting length of the core is roughly the same as in the previous case. Moreover, this is the first instance where we see any clear evidence of a locking of the type discussed in §3 between the two layers. There are many times, for example in the detailed view in figure 9(*a*) as well as near the middle of the sequence in figure 9(*b*), where the vortex spacings in both the inner and outer layers shift to match up in integer ratios. The outer layer appears to do this by delaying vortex ring pairings that would otherwise occur, much as in the delay of vortex pairing in harmonically forced plane turbulent shear layers (e.g. Oster & Wygnanski 1982). When the outer layer vortices then eventually do combine, the resulting interaction often involves more than two vortex rings simultaneously, as in frames 11–18 of the sequence in figure 9(*b*) where three unusually small vortices roll up together in a tripling interaction. This type of interaction occurs frequently, but is intermittent. When it occurs, the resulting dynamics create a deep ingestion of ambient fluid into the potential core. We also note here that the locking seen between the two layers in figure 9 differs substantially from the vortex frequency ratio $F \approx 29$ obtained for this case from the analysis in the Appendix. Instead, the actual frequency ratio is close to two or three. This gives a further indication that the vortex formation and evolution in the two layers do not proceed independently of each other, and that instead disturbances generated by each layer appear to influence the instability and rollup processes in the other layer.

We turn now to figure 10 (Case 5 in table 1) with $U_2/U_1 = 2.56$. Here the inner layer clearly rolls up into shear-layer-like vortices, which now develop quite well before interacting with the shear-layer vortices that form in the outer layer. The resulting shear-layer vortices in the inner and outer layers again have opposing senses of circulation. Here the locking between the two layers is present most of the time. Note, for example in figure 10(*a*), that vortex pairings in the outer layer appear to

(*b*)

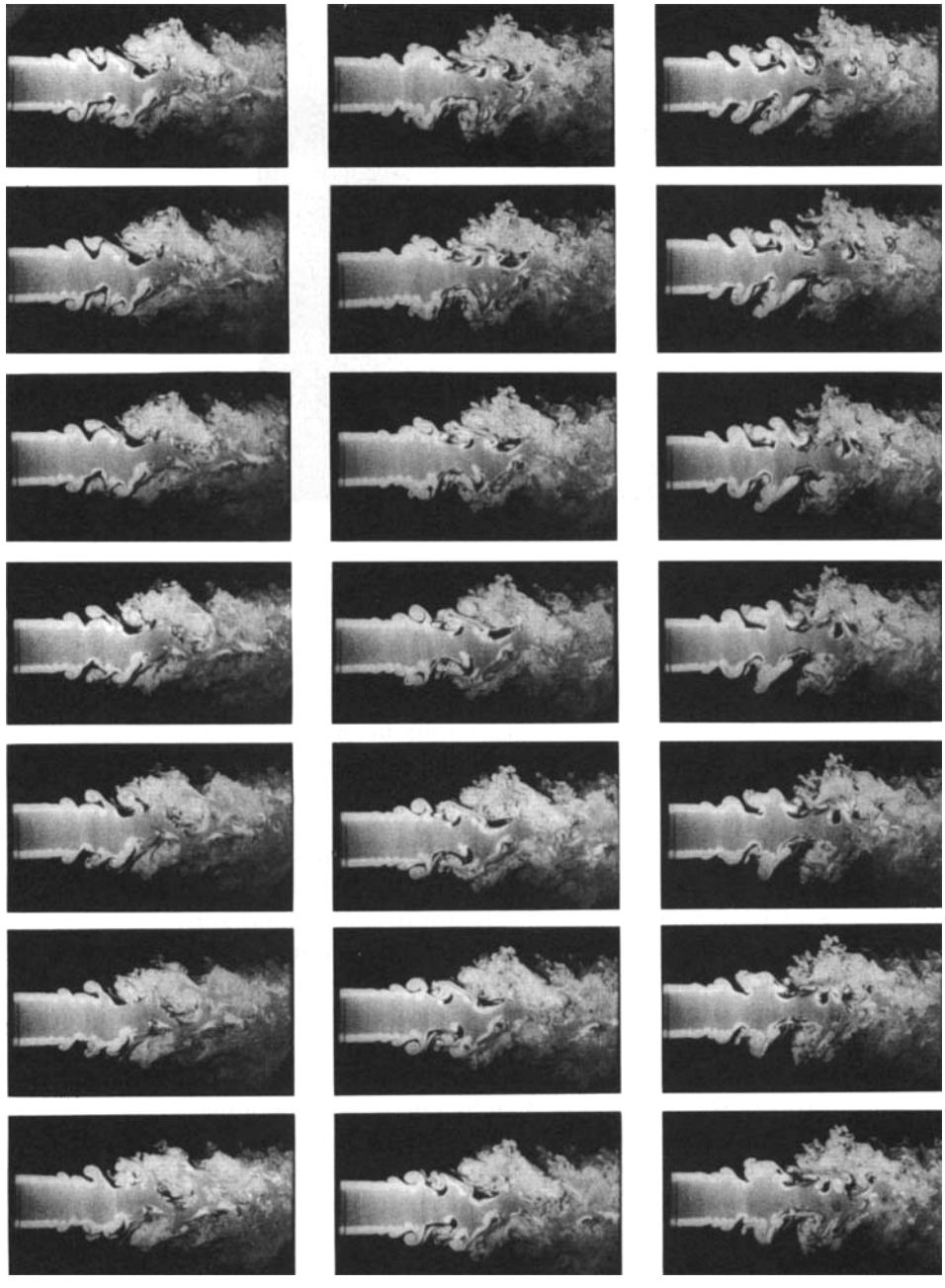

FIGURE 9. Cross-sectional LIF photographs showing the coaxial jet near-field vortex structure and dynamics for $U_2/U_1 = 1.14$ (Case 4 in table 1). The velocity jumps across the inner and outer layers now take on opposing signs, and the first indications of a locking between the two layers becomes evident. As is also the case in figure 8, the apparently increased symmetry is not as effective in disrupting the potential core as in figure 7. (*a*) Typical near-field vortex structure. (*b*) Sequence showing typical vortex dynamics in the near field with time increasing from bottom to top, left to right, as in figure 6(*b*).

(*a*)

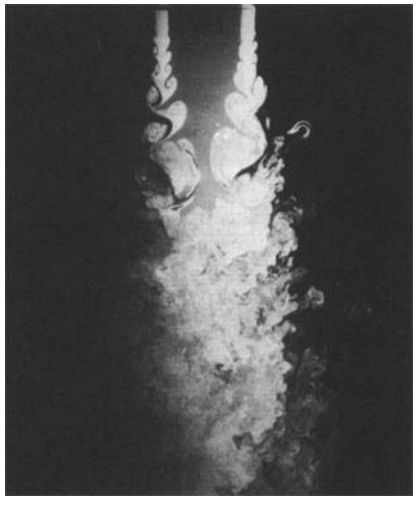

FIGURE 10(*a*). For caption see facing page.

be delayed, instead forming a series of abnormally constant-size vortices. When the vortices in the two layers do interact, it is often through a cycling in which, for example, one vortex from the inner layer rolls up with one vortex from the outer layer, then on the next cycle two vortices from the inner layer will combine with one from the outer layer. The asymmetries which this cycling can introduce are more effective at consuming the potential core than the more symmetric interactions in, say, figures 8 or 9. The core is now regularly torn into the long tentacular features seen in figure 10, and is consistently even shorter than it was in figure 7. Note also that the actual vortex frequency ratio seen in figure 10 again differs substantially from the value $F = 3.2$ obtained in the Appendix for these conditions under the assumption that the shear-layer vortices in the two layers develop independently of each other. This provides some measure of quantitative verification for the observation that the vortices in the two layers lock into each other.

The last case we will examine here is shown in figure 11 (Case 6 in table 1). Now the velocity ratio U_2/U_1 is raised to 4.16 by decreasing the inner stream velocity to 2.5 cm/s. Again the velocity jumps across the inner and outer layers have opposite signs, but now they both have roughly the same magnitude. Both layers can be seen to roll up extensively into well-defined shear-layer-like vortices with opposing senses of circulation and nearly equal strengths. The locking between the two layers is extensive and essentially always present, with the interactions between the layers occurring cyclically as follows. In the first half of the cycle, a vortex from the outer layer rolls a vortex from the inner layer outward and then around itself, while in the second half-cycle a vortex from the inner layer draws a vortex from the outer layer inward and around itself. The first half-cycle produces a long tentacle of inner fluid reaching out toward ambient fluid, while the second produces an intrusion of annular and ambient fluid into the potential core. As a result, the potential core now ends abruptly at about one-and-a-half diameters downstream. Again, the frequency ratio F differs substantially from the value 2.0 obtained for this case in the Appendix. The

(*b*)

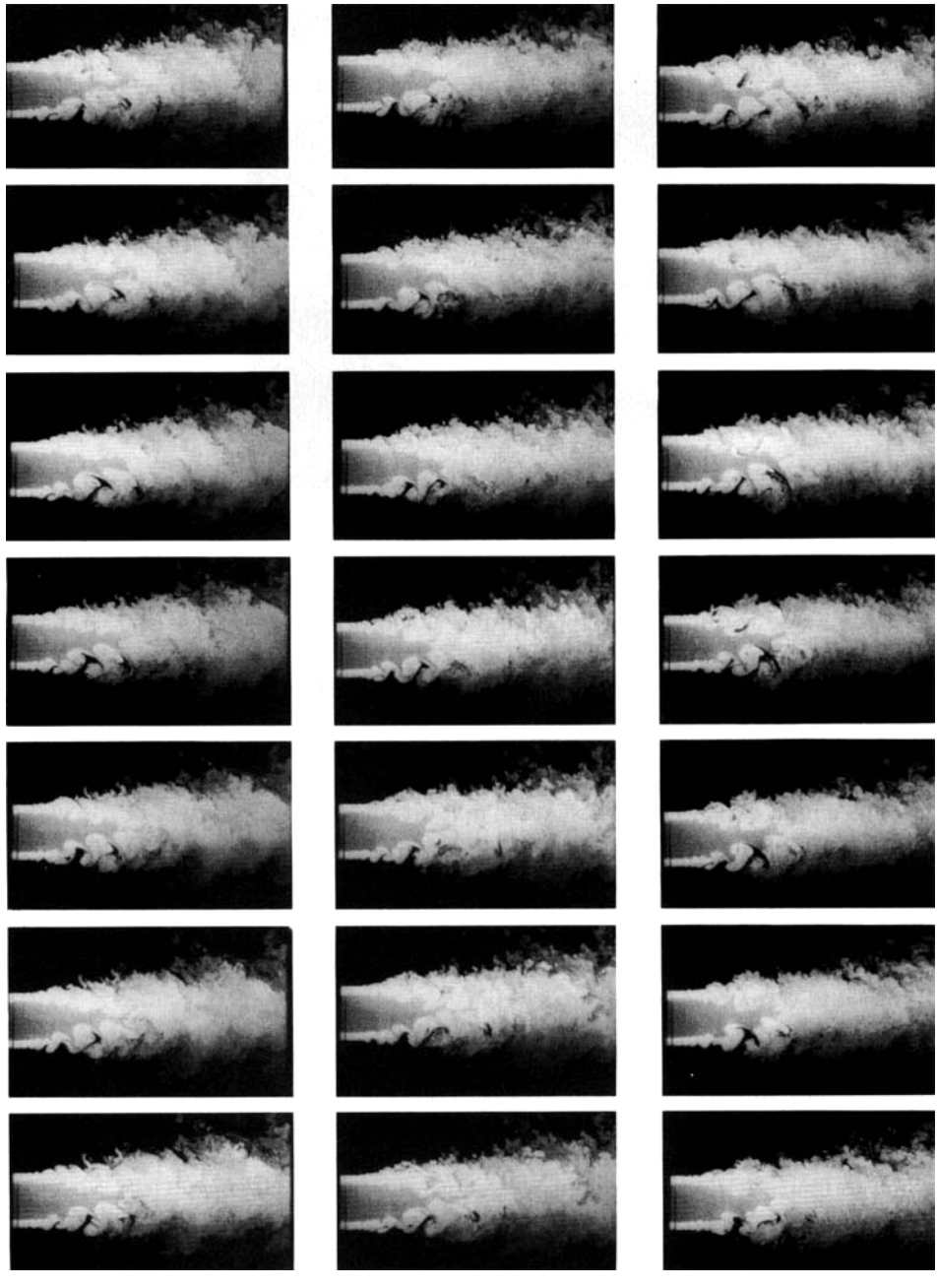

FIGURE 10. Cross-sectional LIF photographs showing the coaxial jet near-field vortex structure and dynamics for $U_2/U_1 = 2.56$ (Case 5 in table 1). Here the inner layer clearly rolls up to form well-developed shear-layer-like vortices with the opposite sense of circulation from those in the outer layer. The locking between the layers is now readily apparent, and produce a cyclic interaction between their vortices that is very effective at disrupting the potential core. (*a*) Typical near-field vortex structure. (*b*) Sequence showing typical vortex dynamics in the near field, with time increasing from bottom to top, left to right, as in figure 6(*b*).

(a)

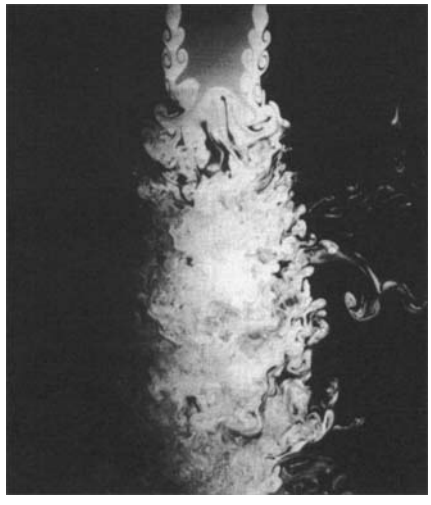

FIGURE 11(a). For caption see facing page.

actual frequency ratio, as described above, is closer to one, suggesting that the two layers do not develop independently.

The results in figures 6–11 show some of the effects of the velocity ratio on the vortex sheet instability and rollup processes that determine the structure and dynamics in the coaxial jet near field. In particular, these results show that a variety of widely differing near-field vortex patterns can arise, with very different interaction dynamics, which depend on the relative magnitudes and thicknesses of the wake and shear-like components of the compound velocity profiles at each nozzle lip. They also show that a locking between the two layers can play an important role in the initial instability and rollup processes, and in the subsequent vortex interaction processes. In the following section, we briefly examine a case in which the absolute stream velocities additionally play an important role in determining the near-field vortex structure and dynamics in the coaxial jet.

4.2. *Effect of absolute velocities*

Figure 12 compares the near-field vortex structure for two cases that each have the *same* velocity ratio $U_2/U_1 = 1.00$ but have different absolute velocities. Specifically, in figure 12(*a*) the two coaxial stream velocities were each 11 cm/s (Case 3 in table 1), while in figure 12(*b*) the streams were both moving at 20 cm/s (Case 7 in table 1). Note that a very different near-field vortex structure is seen in these two cases, despite that fact that both have the same velocity ratio. We also show a time sequence from the ciné film data for Case 7 in figure 13, which should be compared with the corresponding sequence for Case 3 in figure 8(*b*), and demonstrates that the resulting vortex interaction dynamics in the near field also change dramatically as the velocity is increased. While previous investigations of coaxial jets have concentrated almost exclusively on effects of the velocity ratio, figures 12 and 13 suggest that the absolute stream velocities can also play an important role in determining the near-field structure and dynamics.

Specifically, in figure 12(*a*), the wake instability of the inner layer can be clearly

(*b*)

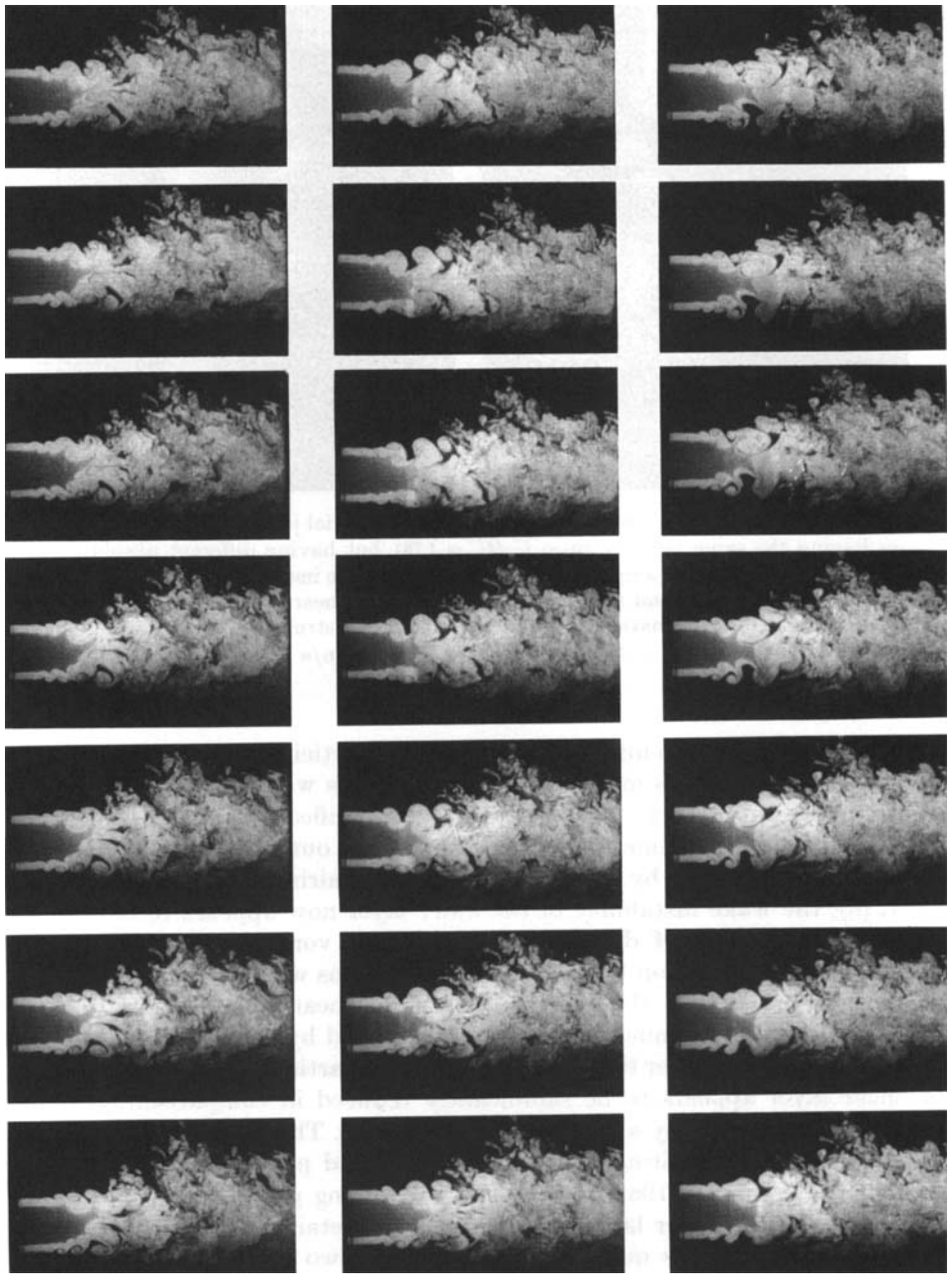

FIGURE 11. Cross-sectional LIF photographs showing the coaxial jet near-field vortex structure and dynamics for $U_2/U_1 = 4.16$ (Case 6 in table 1). The shear-layer-like vortices that form in the inner and outer layers now have nearly equal and opposite circulations and are strongly locked into each other. The cyclic interactions between them now cause the potential core to end abruptly after only one-and-a-half diameters. (*a*) Typical near-field vortex structure. (*b*) Sequence showing typical vortex dynamics in the near field, with time increasing from bottom to top, left to right, as in figure 6(*b*).

(a) (b)

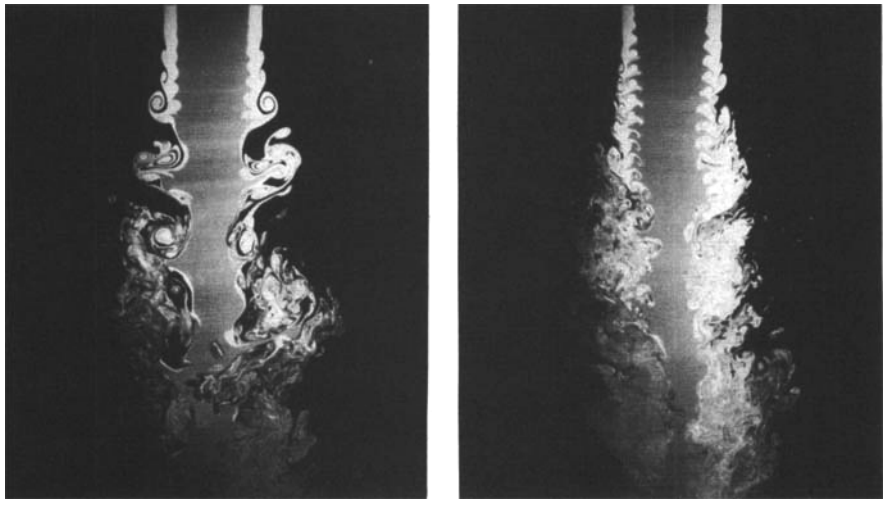

FIGURE 12. Cross-sectional LIF photographs showing the coaxial jet near-field vortex structure for two cases having the same velocity ratio $U_2/U_1 = 1.00$, but having different absolute velocities. Note that, owing to the larger amplification rates for the wake instability of the inner layer in (*b*), the wake vortices that form and their interaction with the shear-layer vortices formed from the outer layer produce a dramatically different near-field structure from that seen in (*a*). (*a*) $U_1 = U_2 = 11$ cm/s (Case 3 in table 1). (*b*) $U_1 = U_2 = 20$ cm/s (Case 7 in table 1).

seen, but does not develop into strongly localized vorticity concentrations before its further evolution becomes mandated by interactions with the shear-layer vortices that form in the outer layer. As a result, the only significant vorticity concentrations are the essentially axisymmetric vortex rings in the outer layer, and the near-field dynamics are dominated by their formation and pairings. On the other hand, in figure 12(*b*), the wake instability of the inner layer now appears to develop into a staggered arrangement of dynamically significant vorticity concentrations with opposing signs of circulation before strong interactions with the outer-layer vortices begin. Equally important, the development of the shear-layer vortices in the outer layer now appears to be much more strongly affected by the evolution of the wake instability in the inner layer than in figure 12(*a*). In particular, the growth rate of the outer shear layer appears to be significantly reduced in comparison with that in figure 12(*a*), apparently by a lack of vortex pairings. This is somewhat reminiscent of the delay of vortex pairing in harmonically forced plane turbulent shear layers (e.g. Oster & Wygnanski 1982), where here the forcing presumably comes from the wake vortices in the inner layer. As a result, the detailed structure of the vortex patterns in both layers is quite different in these two cases, and accordingly the resulting interaction dynamics between vortices in the inner and outer layers are also quite different. A further comparison of figures 8(*b*) and 13 shows that the consequent effects on mixing in the near field, and in particular on the consumption of the potential core, are also different in these two cases.

It appears possible to understand the underlying reason for these differences in the near field by considering the effect of the absolute stream velocities on the wake instability of the inner layer. Referring to figure 5, the growth rate of the wake instability can be expected to increase as the combined thickness δ of the boundary

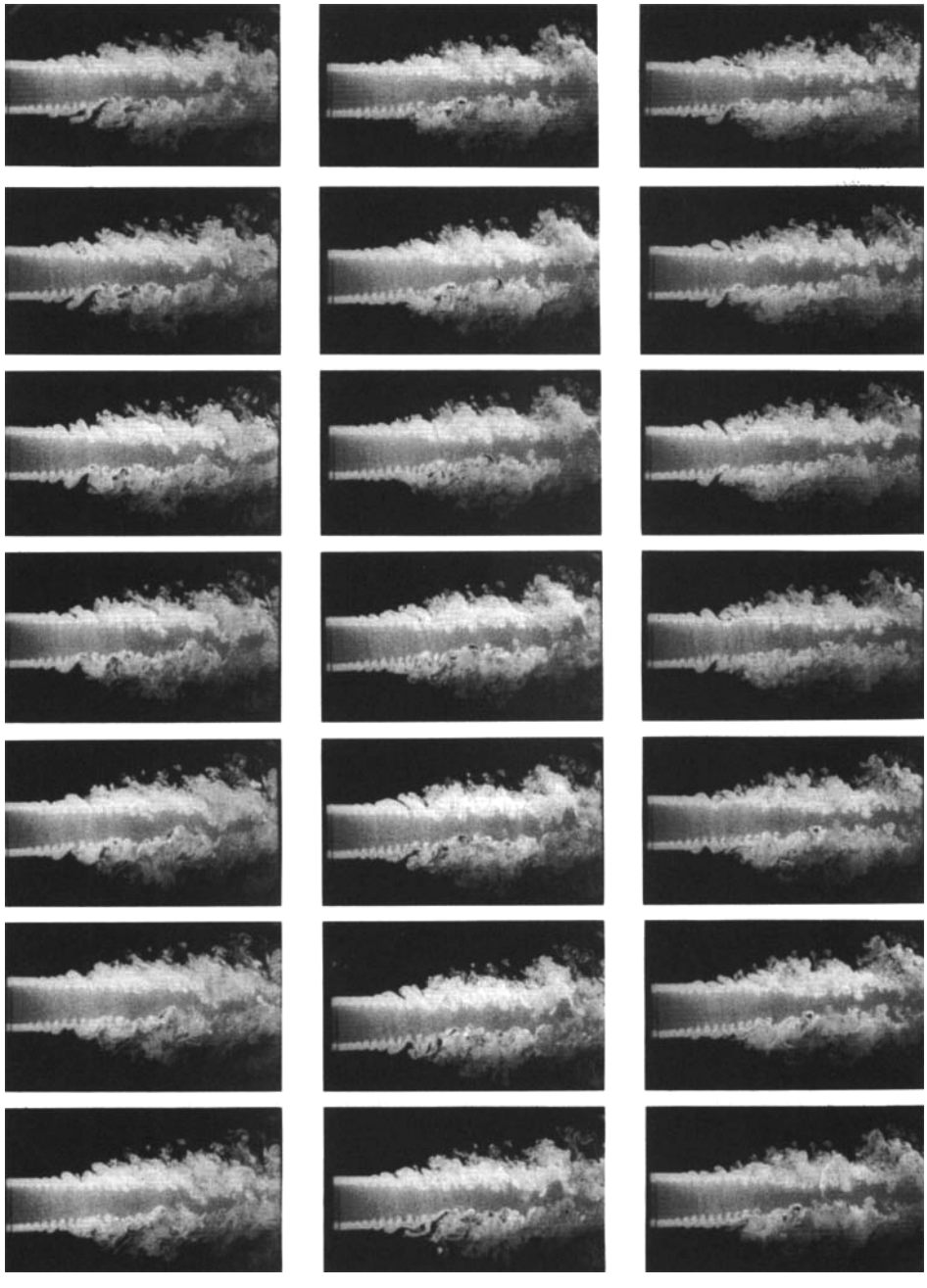

FIGURE 13. A single time sequence showing the typical coaxial jet near-field vortex dynamics for $U_2/U_1 = 1.00$ with $U_1 = U_2 = 20$ cm/s (Case 7 in table 1). Compare with figure 8(*b*) to see how the more extensive development of the wake vortices from the inner layer in this case produces significantly different vortex interactions in the near field, time increases from bottom to top, left to right, as in figure 6(*b*).

layers on either side of the inner nozzle decreases and as the wake defect velocity U increases. Indeed, in going from Case 3 to Case 7, δ decreases by about a third while U increases by a factor of nearly two. This would suggest that the growth rate for the

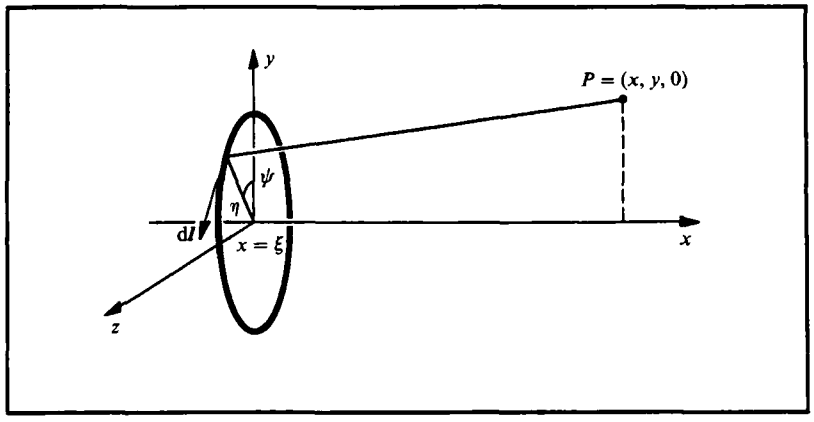

FIGURE 14. Notation used for expressing the velocity induced at a point P due to a single axisymmetric vortex filament.

wake instability of the inner layer is significantly larger in figure 12(*b*) than in figure 12(*a*), and the rollup of the inner interface appears to confirm this. The results in figure 12 suggest that this increase in growth rate allows the inner layer to form its own dynamically significant vorticity concentrations, which subsequently alter the entire evolution of the near-field vortex structure. Furthermore, while dominance of the wake-like instability mode of the inner layer is assured when the velocity ratio is one, for a range of velocity ratios near unity, an essentially wake-like mode would be expected to continue before the shear-layer-like mode becomes dominant. The effect of the absolute velocities on the near-field structure and dynamics seen in figure 12 is unlikely therefore to be limited just to the case where $U_2/U_1 = 1.00$. Of course, with $U_3 = 0$ in all of the cases shown here, the shear-layer mode will always dominate in the outer layer.

4.3. *Numerical simulations*

The experimental results in §4.2 appear to document an effect of the absolute stream velocities on the structure and dynamics of the vortex patterns that form in the near field of a coaxial jet. In this section, we attempt to simulate this phenomenon numerically to assess the explanation offered for the role of the absolute velocities through the thinning of the vorticity layers. In particular, we use an inviscid axisymmetric vortex method to simulate the rollup of the wake and shear-layer modes in the inner and outer layers, and examine some of the effects of the layer thicknesses.

While inviscid vortex methods for two-dimensional flows are well developed, such methods are less common for axisymmetric geometries. To model the evolution of the vortex structures and their dynamics in the near field of a coaxial jet, we follow the approach used in two dimensions and replace the vorticity layers with discrete vortex elements, though using axisymmetric vortex filaments instead of vortex points. The velocity field due to an axisymmetric vortex filament is usually not quoted in classical references (although the stream function is), and it therefore seems useful to outline first the expressions used for the velocities in the time integration. Figure 14 shows a single axisymmetric vortex filament and an arbitrary

point P in the (x, y)-plane. We compute the velocity at P by a direct integration of the Biot–Savart law, namely

$$\boldsymbol{u} = \frac{-\Gamma}{4\pi}\int \frac{\boldsymbol{r}\times \mathrm{d}\boldsymbol{l}}{r^3}.$$

The velocity at P has components (u, v, w), where u is the axial velocity, v the radial component, and w the swirl component which vanishes here. From the figure we can infer that

$$\boldsymbol{r} = (x-\xi, y-\eta\cos\psi, -\eta\sin\psi).$$

and

$$\mathrm{d}\boldsymbol{l} = \eta(0, -\sin\psi, \cos\psi)\,\mathrm{d}\psi.$$

The velocity at P due to a single such vortex filament is therefore

$$(u, v, w) = \frac{\Gamma\eta}{4\pi}\int_0^{2\pi} \frac{\{\eta - y\cos\psi, (x-\xi)\cos\psi, (x-\xi)\sin\psi\}\,\mathrm{d}\psi}{\{(x-\xi)^2 + y^2 + \eta^2 - 2y\eta\cos\psi\}^{\frac{3}{2}}}.$$

After lengthy but straightforward manipulations this expression becomes

$$(u, v, w) = \frac{\Gamma\eta k^3}{\pi(4\eta y)^{\frac{3}{2}}}\int_0^{\pi/2} \frac{\{\eta + y - 2y\sin^2\alpha, (x-\xi)(2\sin^2\alpha - 1), 0\}\,\mathrm{d}\alpha}{\{1-k^2\sin^2\alpha\}^{\frac{3}{2}}},$$

where

$$k^2 = \frac{4\eta y}{(x-\xi)^2 + (y+\eta)^2}.$$

This can be easily rewritten in terms of the complete elliptic integrals of the first and second kinds, $K(k)$ and $E(k)$ respectively, using the fact that

$$\int_0^{\pi/2} \frac{\mathrm{d}\alpha}{\{1-k^2\sin^2\alpha\}^{\frac{3}{2}}} = \frac{1}{1-k^2}E(k),$$

$$\int_0^{\pi/2} \frac{\sin^2\alpha\,\mathrm{d}\alpha}{\{1-k^2\sin^2\alpha\}^{\frac{3}{2}}} = \frac{1}{(1-k^2)\,k^2}E(k) - \frac{1}{k^2}K(k),$$

giving

$$(u, v, w) = \frac{\Gamma\eta k}{\pi(4\eta y)^{\frac{3}{2}}}\left\{\left(\frac{k^2(\eta+y)-2y}{1-k^2}E(k) + 2yK(k)\right), (\xi-x)\left(\frac{k^2-2}{1-k^2}E(k) + 2K(k)\right), 0\right\}.$$

The elliptic integrals can be computed efficiently by a polynomial approximation. The above result can also be derived by starting with the stream function and differentiating.

For a system of such axisymmetric vortex filaments, the velocity at point j is a sum over the contributions from all the vortex rings, giving

$$u_j = \frac{1}{\pi}\sum_{i=1}^{N} \frac{\Gamma_i r_i k_{ij}}{(4r_j r_i)^{\frac{3}{2}}}\left[\left(\frac{(r_i + r_j)k_{ij}^2 - 2r_i}{1-k_{ij}^2}\right)E(k_{ij}) + 2r_i K(k_{ij})\right],$$

$$v_j = \frac{1}{\pi}\sum_{i=1}^{N} \frac{\Gamma_i r_i k_{ij}(x_j - x_i)}{(4r_j r_i)^{\frac{3}{2}}}\left[\left(\frac{k_{ij}^2 - 2}{1-k_{ij}^2}\right)E(k_{ij}) + 2K(k_{ij})\right],$$

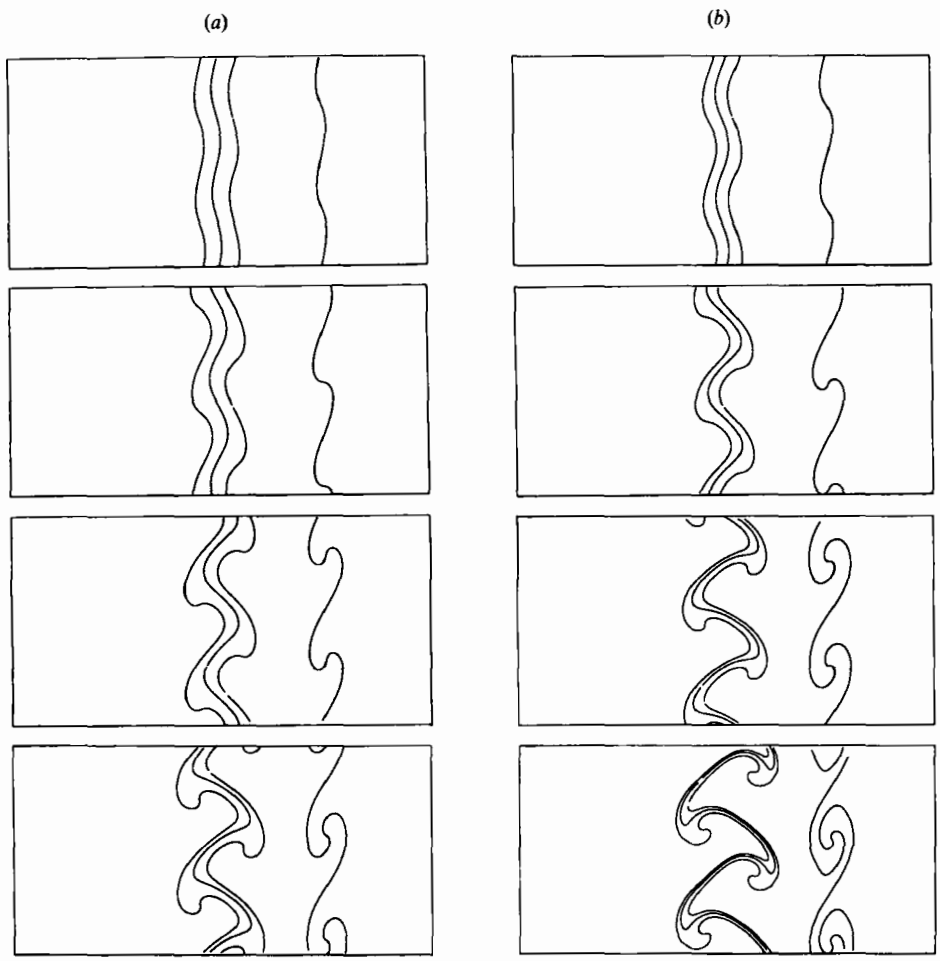

FIGURE 15. Inviscid simulation of the temporal evolution in the near field of a coaxial jet, showing one half of the jet with the left edge of each panel corresponding to the jet centreline. The first, second and fourth lines from the right indicate the centres of vortex layers with non-dimensional strengths $+1:-1:+1$, respectively, producing a velocity jump across the outer layer and a pure wake defect in the inner layer. Parameters including the vorticity-layer thicknesses have been chosen to approximately simulate the conditions in figure 12 (*a*, *b*). The evolution of the resulting near-field structure is shown at non-dimensional times 0.5, 1.0, 1.5, and 2.0. (*a*) Thick layers ($\delta = 0.135$) simulating Case 3 in table 1. (*b*) Thin layers ($\delta = 0.10$) simulating Case 7 in table 1.

where we have put $r_l = \eta$, $r_j = y$, $x_l = \xi$, and $x_j = x$. In this notation

$$k_{lj} = \frac{2(r_l r_j)^{\frac{1}{2}}}{[(r_l + r_j)^2 + (x_j - x_l)^2]^{\frac{1}{2}}}.$$

In order to prevent infinite self-induced velocities, and also to prevent the growth of short-wave instabilities, it is necessary to desingularize the above expressions. Following the vortex blob procedure usually used in two dimensions, we replace k_{lj} by

$$\tilde{k}_{lj} = \frac{2(r_l r_j)^{\frac{1}{2}}}{[(r_l + r_j)^2 + (x_j - x_l)^2 + \delta^2]^{\frac{1}{2}}}.$$

While this regularization does not correspond to any real physical effects directly, its influence is somewhat similar to incorporating a finite thickness in the filaments. In the computations presented here, we will vary the δ to model the effect of changing the momentum thickness of each of the axisymmetric vorticity layers.

The computational domain is taken to be periodic in the streamwise direction, and we follow the temporal evolution of the jet rather than the spatial evolution documented experimentally in the previous sections. If the spatial growth of the vorticity layers is sufficiently slow, this calculation approximates the evolution following a point in the flow. To implement the periodic boundary conditions, we have added several 'imaginary' periods to both ends of the computed domain by repeating the vortex configuration in the domain shown. In calculating the velocity of any vortex filament in this domain, we include also the induced velocities from these other periods. Generally we have found it sufficient to keep only a modest number of additional periods. The actual number depends on the radius of the jet, and in the calculations presented here we used 10 periods on either end. Changing this number gave results indistinguishable from those shown here.

Figure 15 shows the resulting near-field evolution of a coaxial jet as calculated by the axisymmetric vortex blob method described above. The configurations shown here are intended to simulate the conditions in figure 12 (*a*, *b*), corresponding to Cases 3 and 7 in table 1, where the effect of the wake between the inner and outer streams is dominant. We therefore used three regularized axisymmetric vortex sheets with relative strengths $+1:-1:+1$ to model the near field. The evolution of the resulting near-field structure is shown at non-dimensional times of 0.5, 1.0, 1.5 and 2.0, with the left edge of each panel shown corresponding to the centreline. The first, second and fourth lines from the right of each panel mark the centres of the vortex layers, so this arrangement produces a shear-layer velocity jump across the outer layer and a pure wake defect with no net velocity jump across the inner layer. The third line from the right of each panel is a set of passive marker particles tracking the interface between the inner and outer streams, and effectively simulating the dye interface in the experiments. The right-most line in each panel also marks the dye interface between the outer and ambient streams, as in the experiments. The vortex layer positions and thicknesses in figure 15 (*a*, *b*) have been chosen to approximately reflect the vorticity-layer characteristics in figure 12 (*a*, *b*) as given in table 1. In particular, to simulate the thicker vorticity layers resulting from the lower absolute velocities in Case 3, in figure 15 (*a*) all the vortex layers are comparatively thick, with regularization scale $\delta = 0.135$, and the two vortex layers representing the wake defect in the inner layer are correspondingly widely spaced. In figure 15 (*b*), the regularization parameter has been reduced to $\delta = 0.10$ and the inner layer spacing decreased correspondingly, in accordance with the thinning of the vorticity layers that results from the higher stream velocities in Case 7. The axisymmetric vortex sheets are initially given a small periodic perturbation, and as this perturbation grows the outer layer rolls up to form vortices typical of the shear-layer mode. The inner layers, on the other hand, can be seen to begin to develop into a wake-like mode, where vorticity concentrations with opposing signs of circulation accumulate in a staggered array. Since our frame of reference is fixed to the stationary ambient stream, these vortices move down in figure 15 under their induced velocities.

The relevant comparisons here are between figures 15 (*a*) and 15 (*b*), and between figures 12 and 15. The former clearly shows the effects of the absolute stream velocities on the development of vortex structure in the coaxial jet near field. In particular, the thinner vorticity layers in figure 15 (*b*) can be seen to lead to a faster

rollup of both the shear-layer mode in the outer layer and the wake mode in the inner layer in comparison with figure 15(*a*). The relatively long time required for such accurate axisymmetric computations precludes tracking the development to much larger times, at which the shear-layer- and wake-like modes will begin to interact. However, even over the time span shown, the operative differences between these two cases can be seen. Moreover, a comparison between figures 12 and 15 shows that the inviscid vortex simulations rather accurately reproduce the effects seen experimentally. Both the wake and shear-layer rollup are seen to occur much more rapidly in figure 12(*b*), corresponding to the thinner vorticity layers. In the experiments, the effects of this more rapid rollup in the inner and outer layers were seen to lead to a significant change in the interaction dynamics further downstream. The simulations thus lend support to the observations in the previous section that not only the velocity ratio, but also the absolute velocities, can play a role in determining the vortex structure and dynamics through their direct effect on the vorticity-layer thicknesses, and thereby their indirect effect on the degree of rollup in the inner and outer layer and the subsequent dynamical interactions between the resulting vorticity concentrations in these layers.

5. Concluding remarks

The results presented here give a detailed view of the vortex structure and dynamics of the near field in a coaxial jet. In contrast with previous indirect investigations based on measurements of averaged velocity profiles and turbulence quantities, which yield a limited type of information about the flow from which it is difficult to infer the detailed characteristics of the underlying vorticity field, these results allow direct observation of the structure of the vortex patterns that form in the jet near field and the dynamics of their subsequent interactions. We note first that the vortex patterns and dynamics observed here are very different from the picture proposed by Ko & Kwan (1976) and Kwan & Ko (1977). In particular, we find no way to usefully reconcile our direct observations with their overall conclusion that the vortex structure of the coaxial jet near field 'can be considered simply as a combination of several single jets'. Instead our results show that, even over the limited range of parameters considered here, a wide variety of dramatically differing near-field vortex patterns can arise, with very different interaction dynamics, which can depend both on the velocity ratio and on the absolute velocities of the two coaxial streams. This structure of the coaxial jet is at least qualitatively understandable in terms of the instability and rollup of the vorticity layers separating each of the three streams. In particular, our results show that in addition to the velocity jump across each of these layers, an accounting of the layer thicknesses and of the wake defect within each layer are essential to an understanding of the evolution of these vorticity layers and the resulting near-field structure of the jet. We see that the vortices that evolve from each layer can be shear-layer-like or wake-like, and either axisymmetric or helical. We also see strong indications of a 'locking' that takes place between the development of the two layers, in which the instability, roll-up and vortex interaction processes within each layer do not proceed independently, but rather appear to be strongly coupled to similar processes occurring in the other layer. One manifestation of this locking is that the vortex passage frequency ratio F, which would appear to be among the most important quantities in determining the near-field dynamics, differs in many cases dramatically from the value predicted by a simple analysis assuming that the two concentric

layers develop independently of each other. Collectively, our results suggest that an understanding of the flow in the near field of such coaxial jets may benefit from a more detailed examination of the underlying vortex structure of the flow than has been attempted previously. Moreover, the connection of the vortex structure with the stability characteristics of the vorticity layers issuing from the nozzle exit provides a meaningful framework for understanding how the near-field structure originates and, further, for potentially simulating it via vortex dynamics calculations of the type demonstrated here that take into account the wake defect in each layer.

These differing vortex patterns and their dynamics also show significant differences in the extent of mixing in the coaxial jet near field. In particular, we note that in figures 6–11 the inner stream velocity is the same, and the changes in the potential core length result entirely from the differing near-field vortex dynamics. These variations in core length are found not to depend simply, or even monotonically, on the velocity ratio of the two coaxial streams as has been suggested by previous studies, but instead show a highly nonlinear dependence on the stream velocities that perhaps is more easily understandable in terms of the near-field vortex patterns and their dynamics than from classical near-field analyses.

Moreover, the observed large-scale vortical structure of the near field as an arrangement of fairly simple vortex rings and helixes suggests that far-field noise formulations based on the vorticity might prove more directly insightful for understanding the noise emission characteristics of such coaxial jets than those based on the more complex resulting velocity field. In particular, Möhring's formulation and his results for the noise produced by individual vortex rings, as well as that generated when two rings pair appear, to be especially relevant. It seems possible that some of the noise reduction characteristics of coaxial jets might be usefully approached, even if only qualitatively, from this perspective. Moreover, this connection between the acoustic far field and the near-field vortical structure of the flow suggests possibilities for eventually gaining some measure of control over the noise generated by such jets through an understanding of their near-field structure and dynamics.

In this connection, it is worth noting that the Reynolds numbers reached by these experiments are necessarily low to allow clear visualizations and maintain accurate control over the jet exit conditions. For the results presented in §4, the overall jet far-field Reynolds numbers are in all cases less than about 15000 and the nozzle boundary-layer Reynolds numbers Re_δ are all below 200. Yet experience in planar shear layers has shown that, once the relevant local Reynolds number is large enough for the layer to become unstable and rollup, the resulting large-scale two-dimensional vortical structure of the flow remains essentially unchanged as the Reynolds number is further increased. It appears likely that this will also remain true for the axisymmetric shear layers in the near field of jets, and that as a consequence the large-scale vortex structures and dynamics seen here at these relatively modest Reynolds numbers will continue to be present even at much higher values of the Reynolds number.

Finally, it may also be possible to infer some of the effects of the three coaxial stream densities on the resulting near-field structure. In particular, the stability calculations by Koochesfahani & Frieler (1989), accounting for the effects of differing densities on the instability and initial rollup of a shear layer with a wake deficit, suggest that as the density ratio departs from unity the shape of the vortex sheet rollup can change significantly, and can actually switch from shear-layer-like to wake-like even at velocity ratios far from unity. As the present results have

indicated, this can certainly produce very significant changes in the structure of the near-field vortex patterns and their interaction dynamics. It might even be possible that some of the dependence of the noise generated by coaxial jets on the stream temperatures could also be understood from this perspective on the near-field vortical structure and dynamics of the flow.

The experiments were conducted during a summer visit by one of us (W.J.A.D.) at GALCIT, during which the hospitality of P. E. Dimotakis was sincerely appreciated. We also acknowledge his original motivation of the problem and his contributions to the design of the experiments, notably in suggesting the design of the nozzles and the pneumatic drive system. The work at GALCIT was supported, in part, by Boeing Commercial Airplane Co. under Contract PO No. Y-405135-0935.

Appendix. Vortex frequency ratio in parallel shear layers

The coaxial jet near field consists of two concentric cylindrical shear layers, each developing with downstream distance. Referring to figure 4, if the shear-layer thicknesses are small in comparison with their diameters and if the two layers developed at least initially independent of each other, then their resulting vortex spacings $l_{12}(x)$ and $l_{23}(x)$ and their convection speeds $u_{12}(x)$ and $u_{23}(x)$ could be estimated from the scaling laws for a single planar shear layer. Following Dimotakis (1984),

$$l_{ij}(x) \approx 0.68\frac{|U_i - U_j|}{U_i + U_j}x, \quad u_{ij}(x) \approx \frac{U_i\rho_i^{\frac{1}{2}} + U_j\rho_j^{\frac{1}{2}}}{\rho_i^{\frac{1}{2}} + \rho_j^{\frac{1}{2}}}.$$

The frequency at which vortices in each layer pass a fixed point is then $f_{ij} = u_{ij}/l_{ij}$, giving

$$f_{ij} \approx \frac{1.47}{x}\left[\frac{U_i\rho_i^{\frac{1}{2}} + U_j\rho_j^{\frac{1}{2}}}{\rho_i^{\frac{1}{2}} + \rho_j^{\frac{1}{2}}}\right]\left[\frac{U_i + U_j}{|U_i - U_j|}\right].$$

The ratio of these frequencies, $F \equiv f_{12}/f_{23}$, is independent of the downstream location x and, when the densities are equal as in the present experiments, becomes

$$F = \left[\frac{U_1 + U_2}{U_2 + U_3}\right]^2 \frac{|U_2 - U_3|}{|U_1 - U_2|}.$$

Similarly, with the shear-layer vortex circulations scaling like $\Gamma_{ij}(x) \sim (U_i - U_j)l_{ij}(x)$, the ratio of the vortex strengths $G \equiv \Gamma_{12}/\Gamma_{23}$ becomes

$$G = \left[\frac{U_1 - U_2}{U_2 - U_3}\right]^2 \left[\frac{U_2 + U_3}{U_1 - U_2}\right].$$

Adopting the conventionally defined shear-layer speed ratio r, where $0 \leqslant r \leqslant 1$, and recognizing that each layer can have either a positive or negative sense of circulation (positive circulation defined into the page, following a right-handed convention in figure 4), we define

$$r_{12}^{+} \equiv U_1/U_2, \quad r_{12}^{-} \equiv U_2/U_1 \quad \text{and} \quad r_{23}^{+} \equiv U_2/U_3, \quad r_{23}^{-} \equiv U_3/U_2.$$

The frequency ratio F is shown as a function of the two speed ratios in figure 16 for each of the four possible combinations of the sense of circulation. In the present

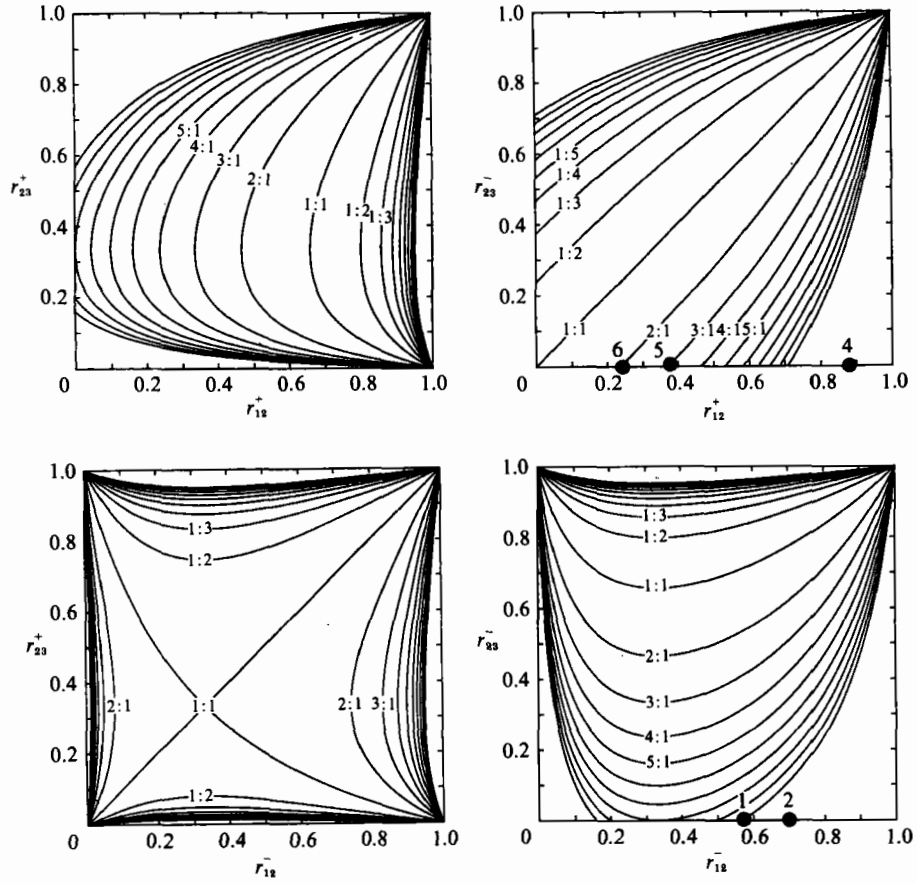

FIGURE 16. The vortex passage frequency ratio F between two independently developing, planar, parallel shear layers as a function of the two speed ratios for each of the four possible combinations of the sense of circulation (see Appendix). The conditions for several of the cases listed in table 1 are also shown in this diagram. Comparisons with the actual vortex frequency ratios observed in figures 6–13 suggests a locking of the instability and rollup processes between the two shear layers that drives the ratio F away from the value for independently developing shear layers (see §3).

experiments, with $U_3 = 0$, the outer layer in all cases has a negative sense of circulation with speed ratio $r_{23}^{-} = 0$. Each of Cases 1–7 in table 1 are shown in this figure.

REFERENCES

BALSA, T. F. & GLIEBE, P. R. 1977 Aerodynamics and noise of coaxial jets. *AIAA J.* **15**, 1550–1558.

BEAVERS, G. S. & WILSON, T. A. 1970 Vortex growth in jets. *J. Fluid Mech.* **44**, 97–112.

BECKER, H. A. & MASSARO, T. A. 1968 Vortex evolution in a round jet. *J. Fluid Mech.* **31**, 435–448.

CHAMPAGNE, F. H. & WYGNANSKI, I. J. 1971 An experimental investigation of coaxial turbulent jets. *Intl J. Heat Mass Transfer* **14**, 1445–1464.

CHAN, W. T. & KO, N. M. W. 1978 Coherent structures in the outer mixing region of annular jets. *J. Fluid Mech.* **89**, 515–533.

CHIGIER, N. A. & BEER, J. M. 1964 The flow region near the nozzle in double concentric jets. *Trans. ASME* D: *J. Basic Engng* **86**, 797–804.

CROW, S. C. & CHAMPAGNE, F. H. 1971 Orderly structure in jet turbulence. *J. Fluid Mech.* **48**, 547–591.

DIMOTAKIS, P. E. 1984 Two-dimensional shear layer entrainment. *AIAA J.* **24**, 1791–1796.

DOSANJH, D. S., YU, J. C. & ABDELHAMID, A. N. 1971 Reduction of noise from supersonic jet flows. *AIAA J.* **9**, 2346–2353.

HOWE, M. S. 1975 Contributions to the theory of aerodynamic noise, with application to excess jet noise and the theory of the flute. *J. Fluid Mech.* **71**, 625–673.

KO, N. M. W. & CHAN, W. T. 1978 Similarity in the initial region of annular jets: three configurations. *J. Fluid Mech.* **84**, 641–656.

KO, N. M. W. & CHAN, W. T. 1979 The inner region of annular jets. *J. Fluid Mech.* **93**, 549–584.

KO, N. W. M. & KWAN, A. S. H. 1976 The initial region of subsonic coaxial jets. *J. Fluid Mech.* **73**, 305–332.

KOOCHESFAHANI, M. M. & FRIELER, C. E. 1989 Instability of nonuniform density free shear layers with a wake profile. *AIAA J.* **27**, 1735–1740.

KWAN, A. S. H. & KO, N. W. M. 1977 The initial region of subsonic coaxial jets. Part 2. *J. Fluid Mech.* **82**, 273–287.

LIGHTHILL, M. J. 1952 On sound generated aerodynamically. I. General theory. *Proc. R. Soc. Lond.* A**211**, 564–587.

LIGHTHILL, M. J. 1954 On sound generated aerodynamically. II. Turbulence as a source of sound. *Proc. R. Soc. Lond.* A**222**, 1–32.

LIGHTHILL, M. J. 1963 Jet noise. *AIAA J.* **1**, 1507–1517.

MATTINGLY, G. E. & CRIMINALE, W. O. 1972 The stability of an incompressible two-dimensional wake. *J. Fluid Mech.* **51**, 233–272.

MICHALKE, A. 1964 On the inviscid instability of the hyperbolic-tangent velocity profile. *J. Fluid Mech.* **19**, 543–556.

MICHALKE, A. & HERMANN, G. 1982 On the inviscid instability of a circular jet with external flow. *J. Fluid Mech.* **114**, 343–359.

MIKSAD, R. W. 1972 Experiments on the nonlinear stages of free-shear-layer transition. *J. Fluid Mech.* **56**, 695–719.

MÖHRING, W. 1978 On vortex sound at low Mach number. *J. Fluid Mech.* **85**, 685–691.

OLSEN, W. A. & FRIEDMAN, R. 1974 Jet noise from coaxial nozzles over a wide range of geometric and flow parameters. *AIAA Paper* 74–43.

OSTER, D. & WYGNANSKI, I. 1982 The forced mixing layer between parallel streams. *J. Fluid Mech.* **123**, 91–130.

POWELL, A. 1964 Theory of vortex sound. *J. Acoust. Soc. Am.* **36**, 177–195.

RIBEIRO, M. M. & WHITELAW, J. H. 1980 Coaxial jets with and without swirl. *J. Fluid Mech.* **96**, 769–795.

TANNA, H. K. & DEAN, P. D. 1975 The effect of temperature on shock-free supersonic jet noise. *J. Sound Vib.* **39**, 429–460.

WHITE, F. M. 1974 *Viscous Fluid Flow.* McGraw-Hill.

WILLIAMS, T. J., ALI, M. R. M. H. & ANDERSON, J. S. 1969 Noise and flow characteristics of coaxial jets. *J. Mech. Engng Sci.* **2**, 133–141.

WLEZIAN, R. W. & KIBENS, V. 1985 Noise-related shear-layer dynamics in annular jets. *AIAA J.* **23**, 715–722.

YULE, A. J. 1973 Large scale structure in the mixing layer of a round jet. *J. Fluid Mech.* **89**, 413–532.